Physics – Uspekhi **47** (6) 583 – 599 (2004)

INSTRUMENTS AND METHODS OF INVESTIGATION PACS numbers: 02.30.Yy; 41.60.Bq; 84.40.Fe

Vavilov – Cherenkov amplifiers with irregular electrodynamic structures

Yu V Gulyaev, V F Kravchenko, A A Kuraev

DOI: 10.1070/PU2004v047n06ABEH001748

Contents

Abstract. Optimal control theory-based methods for improving the efficiency of Cherenkov microwave amplifiers with irregular electrodynamic structures are reviewed. The physics of optimal processes in amplifiers and oscillators with Cherenkov- and combined-type interactions is discussed.

1. Introduction

The Vavilov – Cherenkov effect is known to mean the emission of light in the motion of charged particles through a substance when their velocity exceeds the phase velocity of light waves in this medium [1 – 7]. The same effect is also observed in the motion of charged particles (for instance, electrons) in an artificial quasiperiodic medium formed by quasiperiodic electrodynamic structures. A waveguide with a quasiperiodic boundary can be used as such a structure. The radiation effect arises when the electron velocity exceeds the phase velocity of the spatial harmonic of the field excited in the electrodynamic field structure. This effect underlies the mechanisms of generation and amplification of electromagnetic waves by the electron current in traveling-wave tubes (TWTs) and backward-wave tubes (BWTs) — "Cherenkov" amplifiers and oscillators. It would be well to refer to them as Vavilov – Cherenkov devices, but a simpler term has received acceptance in the international scientific literature — Cherenkov devices. The amplification and generation of electromagnetic waves in such devices relies on the coherent radiation by electrons grouped in phase bunches under the action of the field excited in the electrodynamic system. It is significant that the phase velocity of the synchronous wave decreases due to the reactive component of the interaction, and therefore, unlike in the classical case, Cherenkov radiation also emerges when the electron velocity is lower than the 'cold' phase wave velocity in the system (the phase velocity in the absence of the electron current). Naturally, this effect is taken into account in the self-consistent TWT theory.

The difference between the cold phase velocity and the average electron velocity in the electron flow is the controlling factor of the interaction process in the TWT: its variation along the interaction region makes it possible to significantly vary the conditions of electron phase bunching and the conditions of energy exchange between the electron bunches and the field excited in the electrodynamic system. The variation of the local phase velocity value is determined by the corresponding profile variation of the electrodynamic structure. Therefore, for the realization of interaction control, this structure has to be irregular. The TWT electrodynamic structure profile can be optimized for maximum efficiency using the methods of nonlinear optimal control. The results in this paper were obtained on the basis of a high-efficiency variational-iterative method, the essence of which is described in the Appendix.

Electron motion in the TWT is assumed to be rectilinear (one-dimensional) — this motion is realized when the longitudinal focusing magnetic field is sufficiently strong. For a finite field strength, the circularly polarized components of

Yu V Gulyaev, V F Kravchenko Institute of Radio Engineering and Electronics, Russian Academy of Sciences
ul. Mokhovaya 11, korp. 7, 125009 Moscow, Russian Federation
Tel. (7-095) 200-5258, (7-095) 203-4793
E-mail: gulyaev@cplire.ru; kravchenko_vf@fromru.com; kvf@pochta.ru
A A Kuraev Belorussian State University of Informatics and Electronics
ul. Brovki 6, 220027 Minsk, Belarus
Tel. (375-17) 239-8498
E-mail: kurayev@gw.bsuir.unibel.by

Received 29 September 2003, revised 29 January 2004
Uspekhi Fizicheskikh Nauk **174** (6) 639 – 655 (2004)
Translated by E N Ragozin; edited by A M Semikhatov

the electromagnetic field may be in resonance with the cyclotron oscillation in the electron beam under the conditions of the normal Doppler effect. In this case, the initially rectilinear electron current takes an azimuth sweep, and under certain conditions all beam electrons describe congruent phase trajectories. A gyroton interaction mechanism is realized, whose efficiency in thin (in comparison with the wavelength) beams approaches 100% [8–12]. But the efficiency declines steeply with increasing the beam thickness. In 'thick' beams, as is shown in Section 6, the combined Cherenkov–gyroton interaction is possible, whereby the efficiency is retained at a rather high level.

2. Design and principle of operation of the tubes with an O-type traveling wave

Since their invention by Kompfner in 1943, tubes with an O-type traveling wave have been used quite extensively as low-, medium-, and high-power broadband amplifiers in radar, radio navigation, and communication systems. The amplification band of a medium-power TWT-O with a spiral slow-wave structure (SWS) amounts to one to two octaves for an output power on the order of 100 W. Modern TWT-Os cover the frequency range from 50 MHz to 500 GHz for output power levels from several milliwatts to several megawatts. The TWT-O design is diagrammed schematically in Fig. 1.

The TWT-O amplification mechanism is based on the interaction between the drift electron flow and the field of the slow electromagnetic wave. This interaction turns out to be efficient when synchronism conditions are fulfilled, i.e., the wave phase velocity v_{ph} and the initial velocity v_e of the axial electron drift are approximately equal. In this case, the phase of the field forces acting on the electron and the phase of the electron bunches produced by their action change only slightly throughout the electron SWS-transit time. As a result, electron bunching and the power of the secondary field excited by the electron bunches in the SWS are continuously accumulated (until the emergence of nonlinear effects), i.e., cumulative interaction effects occur for $v_e \approx v_{ph}$.

Figure 2 schematically illustrates the interaction in the TWT for a perfect synchronism, i.e., for $v_e \approx v_{ph}$. Figure 2a shows the distributions of E_z and I_z, as well as the location of individual electrons at the beginning of the interaction region ($t = t_0$). Because preliminary bunching of the electrons in the flow is absent, they are uniformly distributed along the z axis

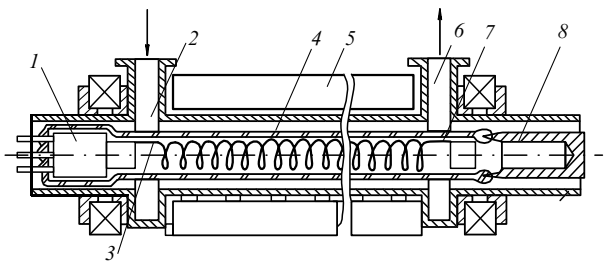

Figure 1. TWT-O design. Electron gun *1* forms a rectilinear electron flow, which passes through the tube axis. Input waveguide *2* is connected to spiral slow-wave structure *4* via pin *3*. The electron beam is focused with magnetic system *5*. Output waveguide 6 is coupled to the spiral SWS with the aid of pin *7*. The waste electron flow is accumulated at collector *8*.

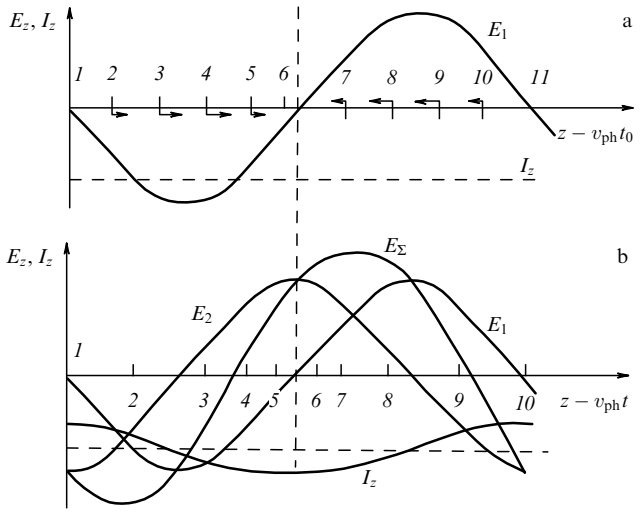

Figure 2. Interaction process in the TWT-O for perfect synchronism at the initial time instant t_0 (a) and for $t > t_0$ (b).

and the current $I_z = \text{const}$. Accordingly, the electrons are uniformly distributed relative to the input wave phase E_1. The forces they experience are determined by the field phase in which the electrons find themselves (the force directions are indicated with arrows). The wave field exerts no action on electrons *1*, *6*, or *11* located at nodes of E_z, while electrons *2–5* are accelerated and electrons *7–10* decelerated by the wave field, the strengths of the accelerating and decelerating forces depending on the electron positions.

The electrons begin to shift under the action of these forces, and at some time instant $t > t_0$, their distribution assumes the shape depicted in Fig. 2b: the electrons are grouped about electron *6*. Therefore, the charge distribution along the beam length becomes nonuniform and there appears a variable current component I_z, which excites the field E_2 in the SWS, phase-shifted by $\pi/2$ relative to the 'primary' field of the input signal E_1. The current now experiences the total field E_Σ, which comoves with the beam, has a higher amplitude than E_1, and is somewhat shifted in phase. In the small signal mode (small electron displacements), the bunching builds up in proportion to the field amplitude and the change of field amplitude is in turn proportional to the bunched current, and the wave field amplitude can therefore be expected to vary by a close-to-exponential law along the z axis.

3. Physical prerequisites for the feasibility of improving the efficiency of a TWT-O with an irregular slow-wave structure

What limits the wave power buildup in the TWT and (which is particularly important for high-power tubes) the efficiency value? With increasing the interaction length or the input signal, nonlinear effects begin to manifest themselves, which limits the wave power. The main nonlinear effects responsible for power saturation in the TWT are as follows: (i) regrouping of the electrons that make up the bunch and the associated decrease of the first harmonic of current in the beam; (ii) deceleration of electron bunches and their escape from synchronism as the energy is being lost (a bunch transition from the decelerating field phase to the accelerating one occurs). Both effects, especially the second one, result in a

significant limitation of the efficiency of broadband TWT-Os, which normally does not exceed 20 – 30%.

At the earliest TWT-O investigation stages, Pierce [13], Slater [14], and others proposed a method for improving the efficiency of energy exchange in the TWT-O by compensating for the effect through a stronger wave moderation towards the tube exit. This method attracted the attention of researchers, and nonlinear calculations of the TWT-O efficiency were subsequently performed with a wave phase velocity varying by the law $v_{\rm ph}(z) \approx v_{\rm e}(z)$ towards the end of the interaction region (see, e.g., Ref. [15]). Such TWT-Os were termed isochronous. However, in-depth investigations of isochronous TWT-Os revealed that applying different isochronism laws to the TWT that operates in the highest-efficiency mode can hardly result in a further rise in efficiency [16].

Another idea for improving the TWT-O efficiency consists in the formation of isophasal conditions at the end of the interaction region: the phase difference between the first harmonic of the beam current and the wave field intensity Δ_φ should be maintained approximately equal to π or selected in some other reasonable way [16]. The calculations in Refs [17, 18] showed that the law of phase velocity variation in the isophasal TWT turns out to be very complicated. In this case, the efficiency of isophasal TWT compared to the efficiency of the uniform tube for sufficiently large values of the gain parameter ε is insignificantly higher (by about 15%).

Therefore, neither method brings about a significant improvement in the TWT-O efficiency, let alone brings it close to 100%. The issue here is that the proposed ways of compensating for the bunch escape from the decelerating phase somewhat impair the conditions for bunching and the focusing of the bunch, which eventually results in its relatively fast 'spreading'.

It is evident that the TWT-O efficiency optimization problem must be solved in a comprehensive manner, i.e., the conditions for energy extraction and for bunching should be improved simultaneously. Indeed, a variation of the phase velocity brings about the variation of the synchronism condition, which may be used to improve the electron bunching conditions (with the main effect consisting in sectioning of the interaction region), as well as the energy extraction conditions (with the additional effect consisting in the formation of isochronism conditions, isophasal conditions, etc.). On the other hand, the transformation and reflection of the co- and counter-propagating waves at irregularities may form a high-frequency (HF) field distribution optimal for the interaction in some frequency band.

Therefore, using the optimal irregular SWS with a large-scale variation of the phase velocity over the entire interaction region (and not only at its end as in isophasal TWTs) it is possible to significantly improve the TWT-O efficiency, which is confirmed by the results given in Sections 4 and 5.

Making full use of the above potentialities for optimizing the TWT-O requires constructing the mathematical model of the interaction between the electron beam and the slow-wave structure. This model should comprise, above all, the equations for irregular SWS excitation, whose derivation in the impedance approximation neglecting losses is given in Refs [17 – 20]. The system of equations that takes the distributed losses in an irregular SWS into account is given in Ref. [21].

4. Efficiency optimization of a TWT-O with a spiral slow-wave structure

In Refs [19 – 21], the law of cold phase velocity variation optimized for efficiency was found and investigated for the first time employing direct optimization for a limited-length TWT-O with different gain parameters ε. The optimal law implies an appreciable increase in the phase velocity over a rather lengthy portion of the interaction region adjacent to the input one. As noted in Refs [17 – 19], in the region where $v_{\rm ph}$ increases, the energy exchange is insignificant, but the reactive interaction is strong, which strongly changes the hot phase velocity $v_{\rm phh}$. At the same time, the bunching in this region, which precedes the isochronous region of energy extraction, is significantly improved in comparison with the bunching in a regular TWT. Unfortunately, this effect did not receive a comprehensive physical explanation in the above papers.

References [22, 23] were concerned with an autophasal TWT-O operating mode, whereby the electrons captured by the traveling wave execute oscillations about the electric intensity node of the wave and slowly give up energy, making it possible to significantly improve the efficiency for a sufficient lengthening of the interaction region.

In the investigation of nonlinear interaction processes in the TWT-O employing the (big)-particle-in-cell method, the authors of Ref. [24] used a somewhat rearranged and simplified system of self-consistent one-dimensional equations from Ref. [17],

$$\frac{{\rm d}\beta_i}{{\rm d}T} = -\varepsilon\theta_0\,\frac{\beta_0^2}{\beta_i}\,(1-\beta_i^2)^{2/3}\left[\sqrt{\rho}\,A\cos(u_i+\vartheta-\Phi)-F_i\right],$$

$$\frac{{\rm d}u_i}{{\rm d}T} = \frac{\theta_0}{\varepsilon}\left(\frac{\beta_0}{\beta_i}-1\right),$$

$$\frac{{\rm d}A}{{\rm d}T} = \sqrt{\rho}\,\frac{2\theta_0}{N}\sum_{i=1}^{N}\cos(u_i+\vartheta-\Phi)-k_{\rm e}\,\frac{\theta_0}{\varepsilon}\,S_T(T)\,A,$$

$$\frac{{\rm d}\vartheta}{{\rm d}T} = -\sqrt{\rho}\,\frac{2\theta_0}{NA}\sum_{i=1}^{N}\sin(u_i+\vartheta-\Phi)$$

with the boundary conditions

$$u_i(0) = \frac{2\pi i}{N}-\frac{\pi}{2}, \quad A(0)=A_0, \quad \vartheta(0)=0, \quad \beta_i(0)=\beta_0.$$

Here, we adopted the notation introduced in Ref. [18]: $u_i = \omega(t-t_{0i}) - h_{\rm e}z$, $i = \overline{1,N}$ is the electron phase trajectory number, ω is the working frequency, t is the time at which the electron transits the section z, t_{0i} is the moment the ith electron enters the interaction region, $h_{\rm e} = k/\beta_0$, $k = \omega/c$, $\beta_0 = v_0/c$, c is the speed of light, and v_0 is the initial electron velocity; $T = z/L$, L is the total length of the interaction region; $\theta_0 = \varepsilon h_{\rm e}L$, ε is the gain parameter defined at the input section, $\varepsilon = (\hat{R}(0)I_0e/2m_0\omega^2)^{1/3}$ is the specific coupling impedance, I_0 is the total electron beam current, e and m_0 are the electron charge and rest mass, respectively; $\rho = \hat{R}(T)/\hat{R}(0)$; $\beta_i = v_i(T)/c$, $v_i(T)$ is the velocity of the ith electron;

$$\dot{A} = A\exp({\rm i}\vartheta) = \frac{e\dot{E}\exp({\rm i}h_{\rm e}TL)}{m_0\sqrt{\rho\varepsilon^2\omega c\beta_0}},$$

A and ϑ are the dimensionless amplitude and phase of the 'hot' wave, respectively, $\dot{E}$ is the longitudinal component of

the electric field of the copropagating wave averaged over the beam section;

$$F_i = \frac{s}{N}\left[\exp(\alpha_i u_i)\sum_{j,\,u_j>u_i}^{u_j<u_j+\pi}\exp(-\alpha_j u_j) - \exp(-\alpha_j u_j)\sum_{j,\,u_j\geqslant u_i-\pi}^{u_j<u_i}\exp(\alpha_j u_j)\right],$$

$s = 2\varepsilon p\exp(2x_0)/(b/a)^2\pi\chi_0^3$, $p = h_e a$, $x_0 = \chi_0 a$, χ_0 is the transverse wave number at the input section, a is the radius of the spiral SWS, b is the radius of the electron flow, $\alpha_j = 2a/pb(1-\beta_j^2)^{1/2}$, $\alpha_i = 2a/pb(1-\beta_i^2)^{1/2}$; Φ is the phase incursion defined by the cold mismatch of the phase velocity $v_{ph}(T)$ and the initial electron velocity v_0 [in the problem involved, $\Phi(T)$ is the interaction process control function]; and

$$S_T(T) = \frac{x^2(T)}{\rho^2\beta_0}\,\frac{0.1205}{W_0}\,\sqrt{f}\,[\text{GHz}],$$

$W_0 = 337$ is the wave impedance of the vacuum, k_e is a coefficient depending on the kind of the spiral material: $k_e = 1$ for a perfectly smooth surface of a copper spiral lead and $k_e > 1$ in reality (in the calculations, it was assumed that $k_e = 2$).

Using the variables introduced, the electron efficiency η_e and the wave efficiency η_w can be written as

$$\eta_e(T) = \frac{1}{N}\sum_{i=1}^{N}\frac{1-R_0/R_i(T)}{1-R_0},$$

$$\eta_w(T) = \frac{\varepsilon\,|\,A^2(T)-A_0^2\,|\,\beta_0^2 R_0}{4(1-R_0)},$$

where $R_0 = \sqrt{1-\beta_0^2}$ and $R_i(T) = \sqrt{1-\beta_i^2(T)}$.

In the presence of distributed losses in the SWS ($S_T \neq 0$), the wave efficiency η_w turns out to be lower than the electron one η_e.

The degree of electron bunching is conveniently estimated by the value of the function

$$G_r(T) = \frac{1}{N}\left[\left(\sum_{i=1}^{N}\cos u_i(T)\right)^2 + \left(\sum_{i=1}^{N}\sin u_i(T)\right)^2\right]^{1/2}.$$

The zero G_r value corresponds to the absence of bunching and $G_r = 1$ to complete bunching.

The results of calculations performed in Ref. [24] were obtained for the following parameter values: the wavelength $\lambda = 10$ cm, $\beta_0 = 0.1$ (the accelerating voltage is $U_0 = 2.57$ kV), $k_e = 2$ (losses of the order of 0.24 cm^{-1} in a regular spiral), the spiral radius $a = 0.31$ cm, the beam radius $b = 0.15$ cm, and $N = 2$.

The main results of the optimization calculations conducted are as follows.

1. If damping is neglected ($S_T(T) = 0$), increasing θ_0 and decreasing ε (i.e., lengthening the interaction region L) results in a monotonic increase in the TWT-O efficiency, which exceeds 90% for $\varepsilon < 0.08$. In this case, the interaction mechanism takes on a typical autophasal character [23]. The cold phase velocity v_{ph} increases in the initial portion of the path, providing retention of the center of the electron phase bunch about the field node of the hot wave, i.e., the hot phase velocity v_{phh} is equal to the initial electron velocity v_0. After the efficient electron bunching, a lengthy energy extraction of the autophasal type begins: the electrons captured by the wave execute limited phase oscillations about the phase of the synchronous electron and are, on the average, slowly decelerated with it. However, the inclusion of damping shows that the wave efficiency decreases drastically and approaches unity in these limiting modes: the autophasal mode is inefficient in the presence of losses.

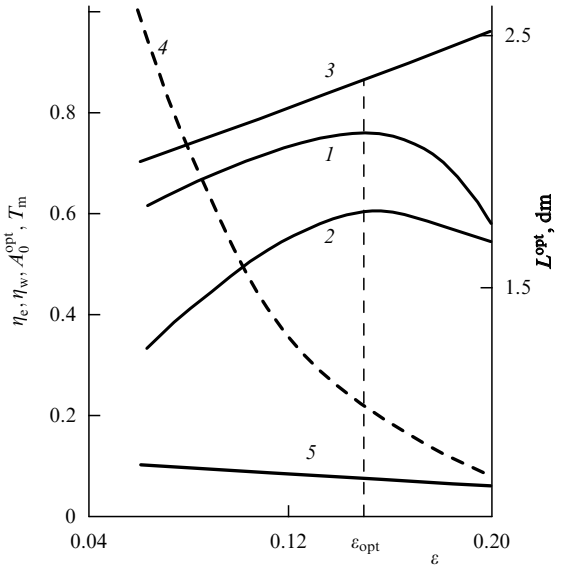

Figure 3. Dependences of the optimized TWT-O parameters on ε for $\theta_0 = 10$: *1* — $\eta_e(\varepsilon)$, *2* — $\eta_w(\varepsilon)$, *3* — $L^{opt}(\varepsilon)$, *4* — $T_m(\varepsilon)$, *5* — $A_0^{opt}(\varepsilon)$.

2. The results of efficiency calculations of the TWT-O optimized with respect to $\beta_{ph}(T)$ for $\theta_0 = 10$ and different ε are given in Fig. 3 in the form of the dependences $\eta_e(\varepsilon)$, $\eta_w(\varepsilon)$, $A_0^{opt}(\varepsilon)$, $L^{opt}(\varepsilon)$, and $T_m(\varepsilon)$, where T_m is the distance at which the first maximum of the bunching function $G_r(T)$ is reached (see Ref. [24]).

As the data suggest, for the given parameters θ_0, k_e, and λ, there exist the optimum values $\varepsilon_{opt} = 0.16$ and $L^{opt} = 1.05$ dm at which η_w reaches its maximum. Decreasing the values of ε results in a sharp rise in the total length of the interaction region L and a shortening of the distance T_m at which the first peak of the bunching function is reached. As a result, the effect of losses in the SWS is substantially enhanced. In particular, the wave efficiency η_w for $\varepsilon = 0.06$, $L = 2.6$ dm, and $T_m = 0.69$ turns out to be two times lower than the electron one η_e, i.e., half the power given up by the electron current is lost in the SWS. When the gain parameter is $\varepsilon > \varepsilon_{opt}$, the limitation of the length L comes into effect: the distance T_m at which the bunching reaches its maximum approaches unity. In particular, the difference between η_w and η_e for $\varepsilon = 0.2$ and $T_m = 0.95$ becomes insignificant, but η_e does not attain a high level. For high ε values, the synchronous-electron method is no longer suited for the description of the TWT-O modes that are almost optimum in efficiency. In this case, advantage should be taken of direct optimization methods, which yield better results [17–21].

Figure 4 gives the TWT-O characteristics $\eta_e(T)$, $A(T)$, $G_r(T)$, $\beta_{ph}(T)$, and $\beta_{phh}(T) = v_{phh}(T)/c$ (where v_{phh} is the phase velocity of the wave under amplification — the hot phase velocity) for the optimum value $\varepsilon = 0.16$ and $\theta_0 = 10$, $A_0 = 0.072$, and $L = 0.99$ dm. These dependences are evi-

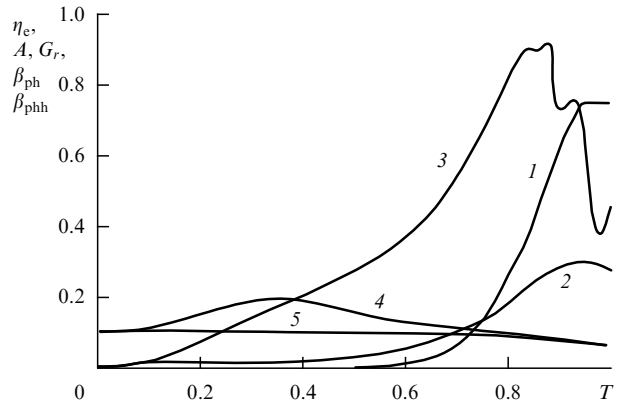

Figure 4. Optimized TWT-O characteristics for the optimum ε: *1* — $\eta_e(T)$, *2* — $A(T)$, *3* — $G_r(T)$, *4* — $\beta_{ph}(T)$, *5* — $\beta_{phh}(T)$.

dence that the interaction mode is not autophasal in this case: $\eta_e(T)$ and $A(T)$ increase monotonically, $G_r(T)$ exhibits one peak, and the energy extraction region is relatively short. It is significant that no active energy exchange is observed (η_e is close to zero) throughout the major portion of the interaction region $0 \leqslant T \leqslant 0.6$, where the bunching function attains a significant magnitude (i.e., the phase bunch is rather well grouped). In this segment, a strong reactive interaction occurs, and retaining the electron bunch in synchronism with the excited wave requires a significant (by nearly a factor of two) increase in the cold wave velocity in the SWS. At the same time, as follows from the plot of $\beta_{phh}(T)$, the hot phase velocity of the excited wave remains invariable and equal to β_0 — the synchronous velocity — throughout the segment $0 \leqslant T \leqslant 0.6$. Analysis of the electron phase trajectories reveals that no electron phase oscillations typical of the autophasal mode are observed in the energy extraction region. The same analysis suggests, on the contrary, that the mode found by the synchronous electron method for $\varepsilon = 0.06$ is typically autophasal: in the energy extraction region, the electrons captured by the wave field execute 2–3 complete phase oscillations.

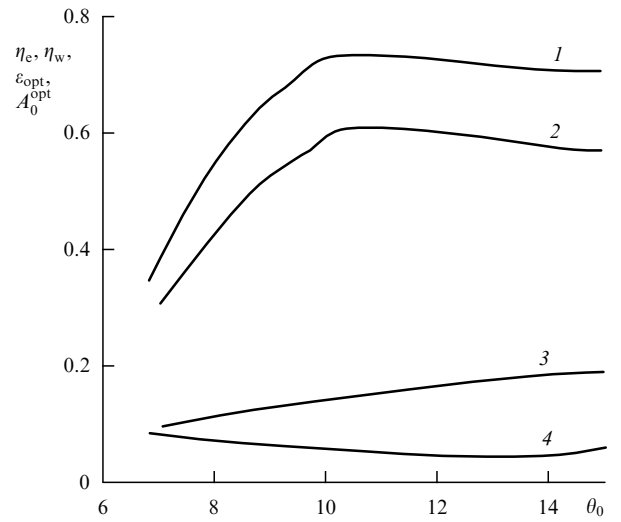

Figure 5. Dependence of the optimum TWT-O parameters on θ_0: *1* — η_e, *2* — η_w, *3* — ε_{opt}, *4* — A_0^{opt}.

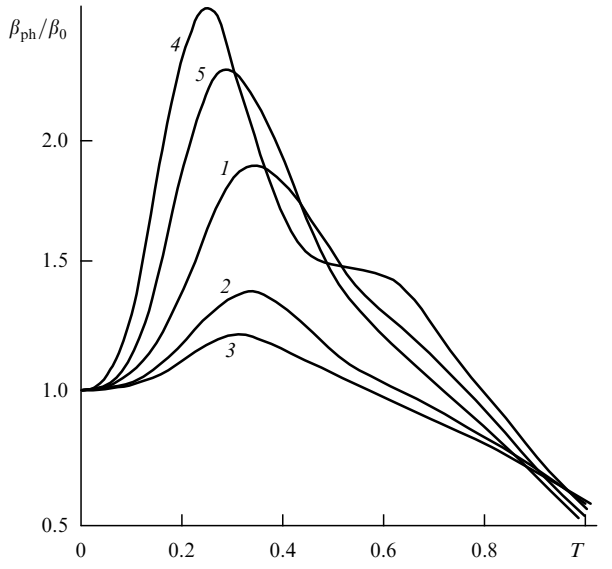

Figure 6. Distribution of the relative phase velocity β_{ph}/β_0 for different optimum versions: *1* — $\varepsilon = 0.16$, $\theta_0 = 10$; *2* — $\varepsilon = 0.0866$, $\theta_0 = 10$; *3* — $\varepsilon = 0.06$, $\theta_0 = 10$; *4* — $\varepsilon = 0.21$, $\theta_0 = 15$; *5* — $\varepsilon = 0.19$, $\theta_0 = 12.5$.

Figure 5 shows the effect of the parameter θ_0 on the optimum characteristics η_e, η_w, ε_{opt}, and A_0^{opt}. We note that the interaction length is nearly constant in the variation range $\theta_0 = 7-15$: $L = 10-11$ cm. This stabilization of the length L is caused by the specified attenuation constant. The lowering of η_e and η_w for $\theta_0 < 10$ occurs because the synchronous electron method does not provide a satisfactory solution of the TWT-O mode optimization problem for small θ_0, as noted above.

Figure 6 shows typical dependences of the relative cold phase velocity $\beta_{ph}(T)/\beta_0$ for different versions optimized for efficiency. The dependences $\beta_{phh}(T)/\beta_0$ not presented here are conventional in character and are similar to those plotted in Fig. 4: the ratio $\beta_{phh}(T)/\beta_0 = 1$ throughout the bunching region and then decreases monotonically in the energy extraction region. As is evident from the above dependences, to maintain this $\beta_{phh}(T)/\beta_0$ variation law, the cold phase velocity $\beta_{ph}(T)$ should rather significantly increase in the bunching region, the magnitude of this increase depending substantially on the gain parameter. The maximum increase of β_{ph}/β_0 for 0.06 is equal to 1.22 and amounts to 2.5 for $\varepsilon = 0.21$. This is related to a drastic strengthening of the effect the electron beam exerts on the characteristics of the excited wave, including the phase velocity, with an increase of the gain parameter ε. The dependences $\beta_{ph}(T)/\beta_0$ for $\varepsilon < 0.19$ are of the same type, the changes occuring only for $\varepsilon = 0.19-0.21$ when the interaction intensity increases sharply.

Figure 7 shows the dynamic characteristic of the optimized TWT-O for $\varepsilon = 0.0866$ and $\theta_0 = 10$. As is evident from Fig. 7, this version of the TWT-O operates as a signal limiter over a rather broad variation range of the input signal amplitude $A_0 = 0.04-0.08$.

The investigation of efficiency-optimized TWT-O modes [24] on the basis of the synchronous electron technique allows making the following conclusions regarding the physical laws of efficiency-optimized interaction processes in the TWT-O.

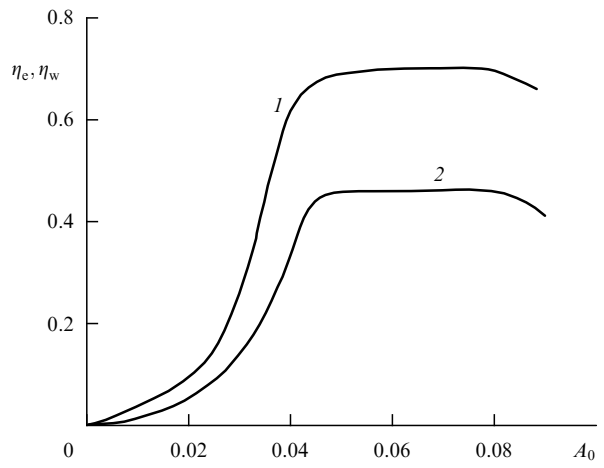

Figure 7. Dynamic characteristics of the optimum TWT: *1* — $\eta_e(A_0)$, *2* — $\eta_w(A_0)$

• The optimum bunching process is realized when two conditions are fulfilled: the hot phase velocity of the wave is equal to the synchronous one v_0 (is close to it in the general case [17 – 21]) and the bunch center is located at the beginning of the decelerating phase near the node of the E_z wave field. When these two conditions are fulfilled, the electron phase bunch moves for a long time in conditions ideally suited for phase focusing (near the node of the focusing forces). Ensuring the fulfillment of these conditions requires increasing the cold wave phase velocity in the bunching region of the SWS. This increase, which is stronger for large gain parameters ε, compensates for the phase shift of the wave field caused by the field component excited by the electron bunches in the SWS (we recall that the bunches move near the node of the total field).

• The energy extraction occurs under conditions close to the isophasal ones; the hot phase velocity of the total wave field monotonically decreases in the extraction region. In this case, two qualitatively different modes may be formed: the relatively fast proceeding mode of monotonic energy extraction, wherein the electrons do not execute phase oscillations (this mode is typical of the TWT-O versions with relatively large ε values, see, e.g., Refs [17 – 21]), and the autophasal mode involving the capture of the phase bunch electrons that oscillate in the potential well of the hot wave and are slowly decelerated, on the average, as this wave moderates [22, 23].

• When distributed losses in the SWS are taken into account, the autophasal mode becomes, as shown by calculations, inefficient owing to the unduly high losses in the extended (in this mode) energy extraction region. To put it another way, the damping in the SWS removes the two-mode 'degeneracy' in the extraction region: only the first mode turns out to be efficient, whereby a fast and monotonic energy extraction from the bunch occurs.

5. Minimization of nonlinear distortions in the frequency band of a TWT-O with an optimized irregular spiral structure

The spectrum of the output signal of a TWT-O contains harmonics of the input signal owing to the nonlinearity of electron bunching. The study of nonlinear signal distortions in the TWT is the objective of Ref. [25] and of several papers whose results are described in monographs [25, 26]. These works were concerned with the investigation of the effect of the ratio between the coupling impedances at the fundamental and higher harmonics, the dispersion, and the missynchronism parameter on the value and character of excitation of higher harmonic components (HHCs) in the regular TWT.

The nonlinear distortions in regular TWTs increase with the improvement in electron bunching and the corresponding rise in efficiency. If an irregular spiral with the optimum pitch variation law is used, the electron efficiency of the TWT may exceed 70% [17, 18]. It would appear reasonable that the nonlinear distortions in such TWTs would also increase. But investigations show [28 – 30] that the HHC fraction in the output signal spectrum of the optimized irregular TWTs is significantly (2 – 3 times) lower than for similar regular TWTs. These investigations, however, were carried out with the same frequency of the input signal ω_0 for which the irregular spiral pitch was optimized.

When the input signal frequency is detuned from the ω_0 frequency, the positions of HHC amplitude peaks may shift along the interaction region, which may result in a variation of the harmonic composition of the output signal. A code package was elaborated for the investigation of these effects on the basis of a more elaborate mathematical model of an irregular spiral TWT. These codes allow optimizing the spiral pitch variation law for maximum efficiency and a minimum nonlinear distortion coefficient in the frequency band.

Mathematical modeling was employed to investigate the effect of higher-harmonic excitation on the amplification efficiency of the optimized irregular TWTs in a frequency band. The resultant characteristic frequency dependences of the nonlinear distortion coefficient K_n for the regular and irregular TWT point to the expedience of employing irregular SWSs for the reduction of nonlinear distortions in the frequency band.

To investigate the nonlinear TWT distortions for a single-frequency (ω) input signal in the stationary mode, we represent the excited field at each section z as the sum of harmonic components $m\omega$. In accordance with the general excitation theory of irregular waveguides described in Refs [17, 18, 28], the longitudinal electric component of the wave field (we consider only the copropagating waves with normal dispersion) averaged over the lateral section of the electron beam is represented as

$$E_{sz} = \sum_{m=1}^{M} E_m(z)\sqrt{\rho_{sm}(z)} \times \cos\left(m\omega t - \int_0^z \frac{m\omega}{v_{\mathrm{ph}\,m}(z)}\,\mathrm{d}z + \vartheta_m(z)\right), \quad (1)$$

where E_m is the amplitude; ϑ_m is the ('hot') phase incursion defined by the field of the electron bunch under formation; $v_{\mathrm{ph}\,m}(z)$ is the ('cold') phase velocity of the natural wave at the $m\omega$ frequency of a regular comparison waveguide corresponding to the section z of the irregular waveguide; $\rho_{sm} = R_{sm}/R_{sm}^0$, $R_{sm} = R_s(z, m\omega)$ is the specific (per unit sectional area) coupling impedance of the natural wave of the regular comparison waveguide at the section z at the $m\omega$ frequency, $R_{sm}^0 = R_s(0, m\omega)$; and $z = 0$ corresponds to the beginning of the interaction region.

In this case, the self-consistent equations that describe the motion of big particles imitating the electron flow in the field

of the excited wave, ignoring damping, are of the form

$$\frac{\mathrm{d}V_i}{\mathrm{d}T} = -\frac{\varepsilon\theta_0}{V_i\gamma_i^3}\left\{\sum_{m=1}^{M}\left[\sqrt{\rho_{sm}(T,W)}\right.\right.$$
$$\left.\left.\times\left(A_{m\,\mathrm{re}}\cos\psi_{mi} - A_{m\,\mathrm{im}}\sin\psi_{mi}\right)\right] - S_q(W)\,F_{qi}\right\},$$

$$\frac{\mathrm{d}u_i}{\mathrm{d}T} = W\frac{\theta_0}{\varepsilon}\left(\frac{1}{V_i} - 1\right),$$

$$\psi_{mi} = m\left[u_i - W\frac{\theta_0}{\varepsilon}\int_0^T\left(\frac{1}{V_{\mathrm{ph}\,m}(T,W)} - 1\right)\mathrm{d}T\right],$$

$$\frac{\mathrm{d}A_{m\,\mathrm{re}}}{\mathrm{d}T} = 2\theta_0\,\frac{R^0_{sm}(W)}{R_{s0}}\left[\sqrt{\rho_{sm}(T,W)}\,\frac{1}{N}\sum_{i=1}^{N}\cos\psi_{mi}\right], \quad (2)$$

$$\frac{\mathrm{d}A_{m\,\mathrm{im}}}{\mathrm{d}T} = -2\theta_0\,\frac{R^0_{sm}(W)}{R_{s0}}\left[\sqrt{\rho_{sm}(T,W)}\,\frac{1}{N}\sum_{i=1}^{N}\sin\psi_{mi}\right],$$

$$i = 1,\ldots,N, \quad m = 1,\ldots,M; \quad V_i(0) = 1,$$

$$u_i(0) = -\frac{\pi}{2} + 2\pi\,\frac{i-0.5}{N}, \quad A_{1\,\mathrm{re}}(0) = A_0,$$

$$A_{1\,\mathrm{im}}(0) = 0, \quad A_{m\,\mathrm{re}}(0) = 0, \quad A_{m\,\mathrm{im}}(0) = 0, \quad m \geqslant 2.$$

The following notation is adopted here: $W = \omega/\omega_0$ is the relative signal frequency, ω_0 is the frequency at which the parameter optimization is performed; $V_i = v_i/v_0$, v_i is the velocity of big particles, v_0 is the average electron velocity at the SWS input; $\gamma_i = 1/(1-\beta_i^2)^{1/2}$, $\beta_i = v_i/c$; $u_i = \omega t - \omega z/v_0$ is the particle phase; $V_{\mathrm{ph}\,m} = v_{\mathrm{ph}\,m}(z, m\omega)/v_0$; $\theta_0 = \varepsilon L\omega_0/v_0$ is the length parameter; $A_{m\,\mathrm{re}} = \mathrm{Re}[A_m\exp(\mathrm{i}\vartheta_m)]$; $A_{m\,\mathrm{im}} = \mathrm{Im}[A_m\exp(\mathrm{i}\vartheta_m)]$; $A_m = eE_m(z)/(m_0\omega_0 v_0\varepsilon^2)$ is the dimensionless amplitude; $\varepsilon = [eI_0R_{s0}/(2m_0\omega_0^2)]^{1/3}$ is the gain parameter; $R_{s0} = R_s(0,\omega_0)$ is the coupling impedance at the reference frequency at the beginning of the SWS; S_q is the space charge parameter, $S_q = 2\varepsilon W\omega_0^2/(\pi\varepsilon_0 cR_{s0}c^2\beta_0^3) = 239.67\varepsilon W\omega_0^2/(\beta_0^3R_{s0}c^2)$, ε_0 is the dielectric constant; F_{qi} is the dimensionless force component of the space charge field exerted on the ith particle by the neighboring particles,

$$F_{qi} = \frac{1}{N}\sum_{k,\,|u_i-u_k|\leqslant\pi} E_q\left(\frac{u_i-u_k}{\pi}\right)\mathrm{sign}(u_i-u_k),$$

where $E_q(x)$ is the dimensionless force component of the charge field exerted on the ith particle by all particles of the electron flow that are separated from it by distances $x\lambda\omega/2 \pm l\lambda_\omega$, $0 \leqslant x \leqslant 1$, $l = 0,1,2,\ldots$; and $\lambda_\omega = 2\pi v_0/\omega$ is the electron wavelength. The function $E_q(x)$ at the frequency ω is calculated by the grid method for a given SWS geometry. The remaining designations correspond to those adopted in Section 4.

The interaction efficiency is determined by the wave efficiency

$$\eta_m = 0.25\,\varepsilon\left[A_m^2(T) - A_m^2(0)\right]\frac{R_{s0}}{R^0_{sm}(W)}\,\frac{\gamma_0+1}{\gamma_0^2},$$

$$\eta_\Sigma = \sum_m \eta_m, \quad (3)$$

where $\gamma_0 = 1/\sqrt{1-\beta_0^2}$.

We estimate the intensity of HHC excitation in terms of the HHC coefficient (HHCC) $K_\mathrm{n} = \sum_{m=2}^{M}\eta_m/\eta_l$, which is characterized by the ratio between the parasitic power and the power of the fundamental signal at the TWT output.

The relative amplitudes of current harmonics at the frequencies $m\omega$ in the bunched electron beam are conveniently characterized by the bunching function

$$G_{rm}(T) = \frac{1}{N}\left[\left(\sum_{i=1}^{N}\cos mu_i(T)\right)^2 + \left(\sum_{i=1}^{N}\sin mu_i(T)\right)^2\right]^{1/2}. \quad (4)$$

Performing calculations with expression (1) requires specifying the dependence of the 'cold' phase velocity $v_{\mathrm{ph}\,m}(z)$ at the frequency $m\omega$ and the dependences of the coupling impedance $R_s(z, m\omega)$ corresponding to a specific SWS for each harmonic.

The coefficients of the system of equations (2) involve an explicit dependence on the relative frequency W. These dependences should also be fixed for a specific SWS when calculating the band characteristics.

To elucidate the main features of HHC excitation, we use the model of a spirally conducting cylinder. In this case, all the requisite frequency characteristics are determined from the well-known dispersion relations [31]

$$x^2\,\frac{\boldsymbol{I}_0(x)\,\boldsymbol{K}_0(x)}{\boldsymbol{I}_1(x)\,\boldsymbol{K}_1(x)} = \left(\frac{\omega}{c}\,R_0\,\mathrm{ctg}\,\chi\right)^2, \quad \frac{\omega^2}{v_{\mathrm{ph}}^2} = \frac{\omega^2}{c^2} + x^2, \quad (5)$$

where χ is the winding angle, R_0 is the spiral radius, $x = k_rR_0$, k_r is the transverse wave number, and $\boldsymbol{I}_0(x)$, $\boldsymbol{I}_1(x)$, $\boldsymbol{K}_0(x)$, and $\boldsymbol{K}_1(x)$ are the modified cylinder functions.

We simplify dispersion equation (5) using the well-known relations for the Bessel functions [32] valid for $x > 1$,

$$\boldsymbol{I}_0(x) \approx \frac{\exp(x)}{\sqrt{2\pi x}}\left(1 + \frac{1}{8x}\right), \quad \boldsymbol{I}_1(x) \approx \frac{\exp(x)}{\sqrt{2\pi x}}\left(1 - \frac{3}{8x}\right),$$

$$\boldsymbol{K}_0(x) \approx \sqrt{\frac{\pi}{2x}}\exp(-x)\left(1 - \frac{1}{8x}\right),$$

$$\boldsymbol{K}_1(x) \approx \sqrt{\frac{\pi}{2x}}\exp(-x)\left(1 + \frac{3}{8x}\right),$$

to obtain the following dispersion equation, which is amenable to calculations:

$$x^2\,\frac{64x^2-1}{64x^2-9} = \left(\frac{\omega}{c}\,R_0\,\mathrm{ctg}\,\chi\right)^2. \quad (6)$$

The coupling impedance at the frequency ω is expressed in terms of the phase velocity by the formula [33]

$$R_s(v_\mathrm{ph},\omega) \approx 183\,\frac{\omega^2}{c^2}\,\beta_{\mathrm{ph}\,\omega}\,k_r^4 \times \exp\left(-2\,\frac{\omega}{c}\,k_rR_0\right)\frac{2}{r_0^2}\int_0^{r_0}\boldsymbol{I}_0^2\left(\frac{\omega}{c}\,k_rr\right)r\,\mathrm{d}r, \quad (7)$$

where $\beta_{\mathrm{ph}\,\omega} = v_\mathrm{ph}(z,\omega)/c$, $k_r = (\beta_{\mathrm{ph}\,\omega}^{-2} - 1)^{-1/2}$, and r_0 is the radius of the electron beam.

We calculate the integral in (7) using the approximate Simpson formula

$$\frac{2}{r_0^2}\int_0^{r_0}\boldsymbol{I}_0^2(ar)\,r\,\mathrm{d}r \approx \frac{1}{3}\left[\boldsymbol{I}_0^2(ar_0) + 2\boldsymbol{I}_0^2\left(\frac{ar_0}{2}\right)\right], \quad (8)$$

where $a = \omega k_r/c$.

The dependences $v_{\mathrm{ph}\,m}(z)$ and $\rho_{sm}(z)$ required in model (2) are unambiguously determined by relations (6) and (7) for a

given variation law of the spiral winding angle $\chi(z)$. In performing calculations, it is expedient to prescribe, in lieu of the law $\chi(z)$, the variation law of the relative phase velocity at the reference frequency $V_{\rm ph}(z) = v_{\rm ph}(z, \omega_0)/v_0$. The $\chi(z)$ function, as well as the dependences $v_{{\rm ph}\,m}(z, m\omega)$ and $R_s(z, m\omega)$ required for the solution of the system of equations (2), is expressed in terms of $V_{\rm ph}(z)$ with the aid of Eqns (6) and (7). As a result, we obtain a closed system of differential equations describing the amplification in the TWT with the inclusion of HHC excitation.

The optimal control problem consists in the derivation of the law $V_{\rm ph}(T)$ that ensures the highest efficiency max $\eta_l(1)$ of the fundamental signal for a minimal value of $K_{\rm n}$. The optimum law $V_{\rm ph}(T)$ is found by the method described in Section 4. For the resultant optimum law $V_{\rm ph}(T)$, we calculate the dependences of the output characteristics η_m and $K_{\rm n}$ on W. It is pertinent to note that the method of calculations described above can also be easily extended to more complex SWS models for which the dependences $V_{{\rm ph}\,m}(V_{\rm ph}(T))$ and $R_{sm}(V_{\rm ph}(T))$ are known. For instance, in Ref. [33], these dependences were obtained for a spiral held in a metal screen using dielectric rods.

All calculations were performed, as in Ref. [30], for the electron beam voltage $U_0 = 5086$ V ($\beta_0 = 0.14$) and the signal frequency $f_0 = 3$ GHz, which corresponds to the wavelength $\lambda_0 = 10$ cm. In this case, for given values of R_0, the model of a spirally conducting cylinder applies. In optimum modes, as shown by the calculations in Ref. [10], the value of the nonlinear distortion coefficient $K_{\rm n}$ for the same interaction length L is primarily determined by the ratio of the coupling impedances at the TWT output ($R_{sm1} = R^0_{sm}/R_{s0}$). The lowering of the fundamental harmonic efficiency with an increase in $K_{\rm n}$ is also observed, although the overall efficiency η_Σ lowers insignificantly. The values of R_{sm1} for a spiral SWS are determined by the parameters R_0, r_0, and $v_{\rm ph}(0)$. Comparison of the optimum versions of the regular and irregular TWTs for approximately the same values of R_{sm1} and L showed that the coefficient $K_{\rm n}$ in the irregular TWT is two times smaller than in the regular one.

To compare the band characteristics of regular and irregular TWTs, we selected the optimum versions for the reference frequency $f_0 = 3$ GHz with the inclusion of the excitation of three parasitic harmonics ($m = 1, \ldots, 4$):

- the regular TWT: $R_0 = 0.22$ cm; $r_0 = 0.18$ cm; $\theta_0 = 7.52$ cm; $\varepsilon_0 = 0.150$; $L = 11.1$ cm; $A_1(0) = 0.018$; $I_0 = 0.30$ A; $V_{\rm ph} = {\rm const} = 0.856$; $\eta_\Sigma = 0.32$; $\eta_m = 0.238$, 0.050, 0.017, 0.009; $R_{sm1} = 1$, 0.808, 0.553, 0.821; $K_{\rm n} = 0.321$; $K_{\rm u} = 40.81$;
- the irregular TWT: $R_0 = 0.25$ cm; $r_0 = 0.20$ cm; $\theta_0 = 9.98$ cm; $\varepsilon_0 = 0.173$; $L = 12.7$ cm; $A_1(0) = 0.115$; $I_0 = 0.62$ A; $V_{\rm ph}$ is variable; $\eta_\Sigma = 0.70$; $\eta_m = 0.632$, 0.042, 0.009, 0.016; $R_{sm1} = 1$, 0.806, 0.536, 0.370; $K_{\rm n} = 0.107$; $K_{\rm u} = 27.98$

The parameters were selected such that the length L corresponds to the first peak of the useful signal power.

The band characteristics for these versions were calculated in the form of the $\eta_m(W)$ and $K_{\rm n}(W)$ dependences with all the parameters and the $V_{\rm ph}(z)$ law fixed equal to those obtained for $W = 1$ (see above).

Figures 8 and 9 show the aforementioned band characteristics for the regular and irregular TWTs, respectively. Analysis of these dependences reveals that the amplification band of the irregular TWT is broader than for the regular one, the efficiency for the fundamental signal for the former being

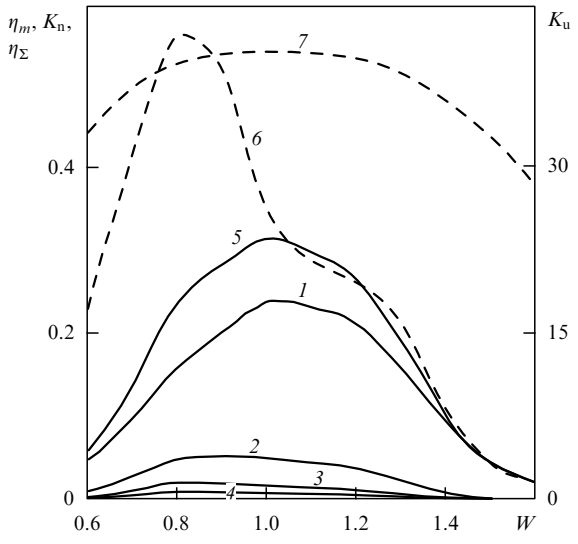

Figure 8. Band characteristics of a regular TWT. Curves *1*–*4* correspond to η_m for $m = 1, \ldots, 4$; curve *5* shows η_Σ; curve *6* represents the dependence of $K_{\rm n}$; curve *7* shows the gain for the fundamental signal $K_{\rm u} = 20 \log A_1(1)/A_1(0)$.

three times higher than for the latter. The regular TWT exhibits a monotonic decrease in the values of η_m towards the band edges. The peak of the mth harmonic power shifts to the low-frequency side as the number m increases. As a result, the nonlinear distortion coefficient $K_{\rm n}$ rises almost twofold for $W = 0.8$.

The dependences $\eta_m(W)$, $m \geqslant 2$, observed for the irregular TWT are oscillatory in character. The magnitude of $K_{\rm n}$ oscillates about a value $K_{\rm n} \approx 0.15$ in the wide segment $0.8 \leqslant W \leqslant 1.5$. Observed only at the low-frequency edge of the amplification band is a steep monotonic increase in $K_{\rm n}$

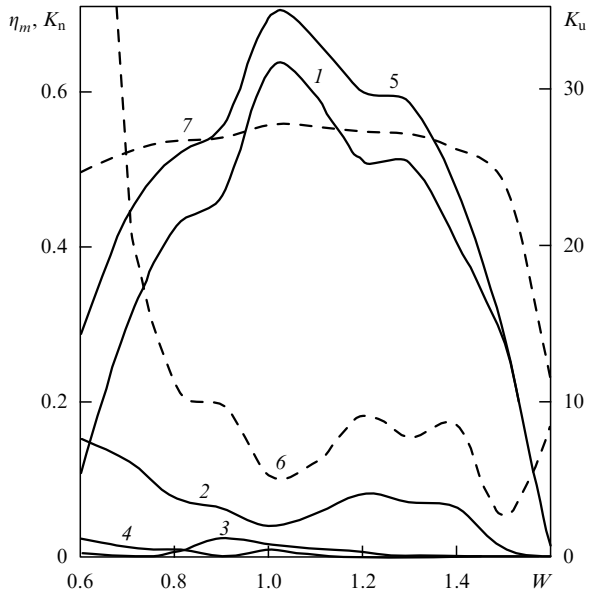

Figure 9. Band characteristics of an optimized irregular TWT. Curves *1*–*4* correspond to η_m for $m = 1, \ldots, 4$; curve *5* shows η_Σ; curve *6* represents the dependence of $K_{\rm n}$; curve *7* shows the gain for the fundamental signal $K_{\rm u} = 20 \log A_1(1)/A_1(0)$.

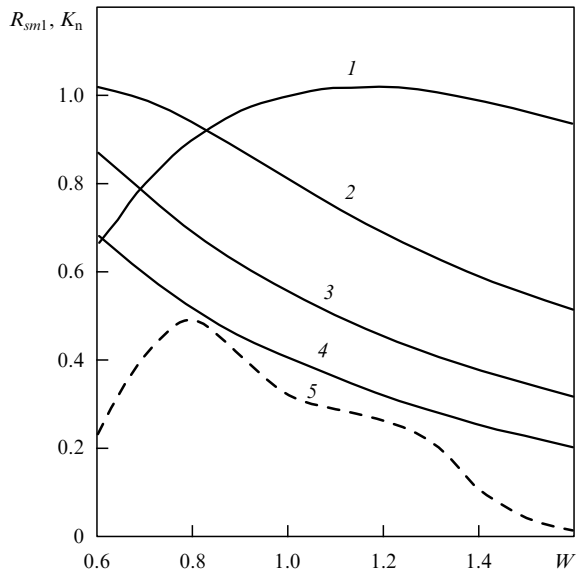

Figure 10. Band characteristics of the regular TWT-O. Curves *1–4* correspond to R_{sm1} for $m = 1, \ldots, 4$; dashed line *5* represents $K_n(W)$.

and a drastic decrease in the useful signal power, with η_2 rising and even becoming greater than η_1. This rise in K_n at the left edge of the amplification band may be explained by the form of the dependences $R_{sm1}(W)$ plotted in Figs 10 and 11 for the regular and irregular TWTs, respectively. The spiral parameters in both versions are selected such that these dependences are virtually the same. The coupling impedance for the fundamental harmonic for $W > 1$ remains on the same level, while the coupling impedances for the parasitic harmonics decrease monotonically. This accounts for the lowering of K_n at the high-frequency edge of the band. The picture for $W < 1$ is different. Here, as W decreases, the coupling impedance for the fundamental harmonic decreases, while for the parasitic harmonics it increases and even exceeds R_{s11}, with the effect that K_n increases. However, in the irregular TWT, K_n monotonically increases with increasing W up to the value of W at which η_1 almost vanishes, but in the regular TWT, K_n reaches its peak and then declines.

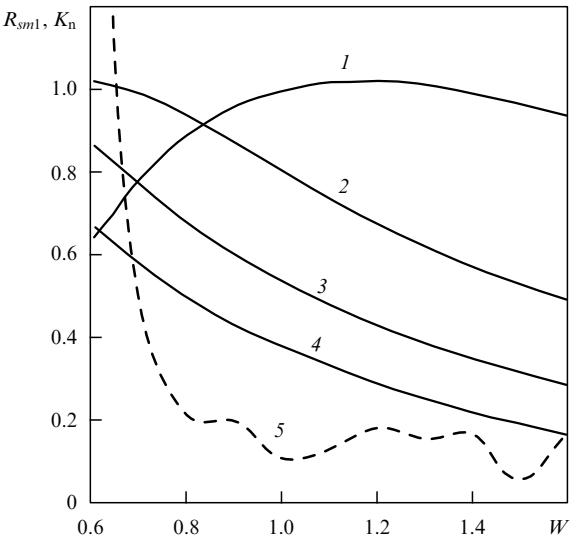

Figure 11. Band characteristics of the optimized irregular TWT-O. Curves *1–4* correspond to R_{sm1} for $m = 1, \ldots, 4$; dashed line *5* represents $K_n(W)$.

Figure 12 shows the variation of the relative coupling impedances $\rho_{sm}(T)$ along the irregular TWT interaction region for different values of W from the amplification band. We note that $\rho_{sm}(T) = \text{const} = 1$ in the regular TWT. Analysis of these curves shows that the spiral pitch variation furnishes an increase in the coupling impedance for the fundamental wave and its simultaneous decrease for the harmonics at the end of the TWT interaction region, where the main electron beam-to-wave energy conversion occurs.

The difference between the coupling impedances for the fundamental and parasitic harmonics varies only slightly for $W > 1$. With decreasing W, this difference rises steeply in the $W < 1$ range, the coupling impedance for the fundamental wave exceeding those for the parasitic harmonics at the end of the TWT interaction region, although it decreases at the beginning of the region (see Fig. 9). This effect accounts for the stabilization of the magnitude of K_n in the irregular TWT for $0.7 \leqslant W \leqslant 1$. The calculations conducted allow concluding that in the irregular spiral TWT, the HHC excitation in the frequency band is suppressed 2–3 times more efficiently than in the regular one owing to the type of dispersion law of the simplest spiral SWS.

6. Traveling-wave gyroton employing a corrugated waveguide

A gyroton [1] of the resonance type [8–10] is a multi-stage amplifier utilizing an initially rectilinear relativistic electron flow (REF). The REF modulation (circular sweep) is effected in rotating fields of the H_{1in}, E_{1in}, or E_{1i0} type excited in sequentially arranged input resonators with the same oscillation types but, unlike in a modulator, under conditions of the electron cyclotron resonance with a standing rotating resonator field or with its concurrent component. An essential element of the resonance gyroton design is the region of transformation of the longitudinal REF velocity to the transverse (modulation) component in the magnetostatic field that grows up to the gyroresonance level. This process largely predetermines the strong dependence of the energy conversion mechanism in the resonance gyroton on the REF thickness. Owing to this, the gyroton efficiency for a given REF diameter declines rather steeply with an increase in the working frequency [10].

In the traveling-wave gyroton (TWG) [11, 12], there is no magnetostatic converter, and the retention of the gyroton phasing mechanism (without phase bunching, all axial electrons are 'correctly phased', and their phase trajectories are congruent) ensures a high efficiency. The TWG should therefore be expected to be less sensitive to the REF thickness and to be a 'higher-frequency' superhigh-power relativistic amplifier.

A TWG employing corrugated waveguide was investigated and optimized in [12] under the assumption that the working wave is the rotating wave EH_{11}, while its related wave HE_{11} is suppressed by special electrodynamic techniques: longitudinal slits or longitudinal grooves of the quarter-

[1] We emphasize that we are dealing with precisely the gyroton and not the gyrotron.

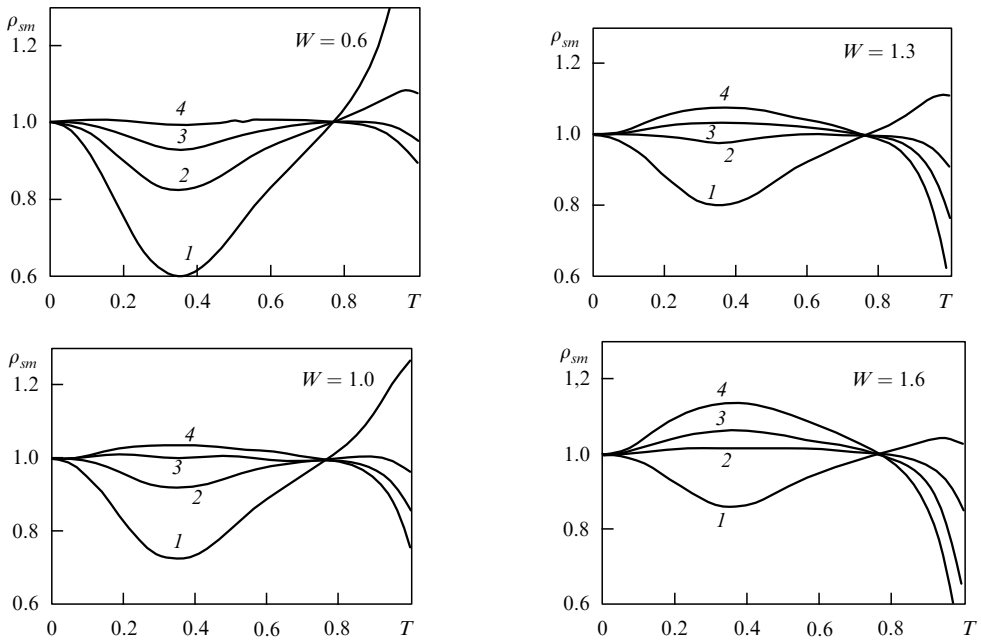

Figure 12. Variation of the relative coupling impedances $\rho_{sm}(T)$ along the interaction region of the irregular TWT for different values of W indicated in the figure.

wave depth. However, these techniques require additional investigation and may prove to be inefficient. Moreover, they may also have an effect on the phase characteristics of the EH_{11} wave. In this section, we therefore consider a TWG in which the REF interacts simultaneously with the coupled HE_{11} and EH_{11} waves of the corrugated waveguide. We show that the ideal gyroton mechanism (for a thin beam) is retained in this situation (i.e., the electron efficiency approaches 100%). Furthermore, we found that the peripheral electrons of a 'thick' REF exhibit a combined mechanism of interaction with the fields HE_{11} and EH_{11} of the corrugated waveguide, which combines the gyroton and Cherenkov interaction mechanisms. That is why considerably 'thicker' REFs can be employed in TWGs than in a conventional gyroton with the retention of relatively high efficiencies. This is attained with the simplest designs with a uniform magnetic field and a regular corrugated waveguide.

We introduce the following simplifications: the space charge fields, the supercritical EH_{1i} and HE_{1i} fields, and the fields of harmonics ω are neglected. In accordance with the general theory of excitation of longitudinally irregular waveguides of circular section [17, 18], the equations for the excitation of the coupled rotating waves HE_{11} and EH_{11} can then be written as

$$\begin{aligned}
\frac{\mathrm{d}\dot{V}_{11}}{\mathrm{d}z} &= \frac{\gamma_{111}^4}{e_{11}}\left\{\dot{A}_{11}^{\mathrm{m}}\left[-\frac{1}{B^2}\left(\frac{\mathrm{d}B}{\mathrm{d}z}\right)^2+\frac{1}{B}\,\frac{\mathrm{d}^2B}{\mathrm{d}z^2}\right]+\frac{\mathrm{d}\dot{A}_{11}^{\mathrm{m}}}{\mathrm{d}z}\,\frac{1}{B}\,\frac{\mathrm{d}B}{\mathrm{d}z}\right\}\\
&\quad-\frac{1}{e_{11}}\left[\dot{A}_{11}^{\mathrm{e}}e_{11}-\left(\frac{\mathrm{d}B}{\mathrm{d}z}\right)^2\dot{A}_{11}^{\mathrm{m}}\gamma_{111}^5\right]\\
&\quad-\frac{1}{N}\sum_{i=1}^{N}\left[\left(\beta_{ri}-\rho_i\beta_{zi}\,\frac{\mathrm{d}B}{\mathrm{d}z}\right)J_1'(\nu_{11}\rho_i)\right.\\
&\quad\left.+\,\mathrm{i}\,\frac{1}{\nu_{11}\rho_i}\,J_1(\nu_{11}\rho_i)\,\beta_{\varphi i}\right]\frac{\exp\left[\mathrm{i}(\varphi_i-T_i)\right]}{\beta_{zi}}\,,
\end{aligned}$$

$$\begin{aligned}
\frac{\mathrm{d}\dot{A}_{11}^{\mathrm{e}}}{\mathrm{d}z} &= \dot{V}_{11}\left(1-\frac{\nu_{11}^2}{B^2}\right)-\frac{\nu_{11}}{b\,e_{11}B^2}\,\frac{\mathrm{d}B}{\mathrm{d}z}\;\dot{A}_{11}^{\mathrm{m}}\gamma_{111}^3\\
&\quad-\frac{\nu_{11}}{e_{11}B}\,\frac{\mathrm{d}B}{\mathrm{d}z}\,\dot{A}_{11}^{\mathrm{m}}\gamma_{111}^{-3}\\
&\quad-\mathrm{i}\,\frac{\sigma\nu_{11}}{\pi b^2e_{11}}\,\frac{1}{N}\sum_{i=1}^{N}J_1(\nu_{11}\rho_i)\exp\left[\mathrm{i}(\varphi_i-T_i)\right],
\end{aligned}\tag{9}$$

$$\begin{aligned}
\frac{\mathrm{d}\dot{P}_{11}}{\mathrm{d}z} &= -\dot{A}_{11}^{\mathrm{m}}\left\{\left[1+\left(\frac{\mathrm{d}B}{\mathrm{d}z}\right)^2\right]-\frac{\mu_{11}^2}{B^2}-\frac{\gamma_{s11}^5}{B^2}\left(\frac{\mathrm{d}B}{\mathrm{d}z}\right)^2\right.\\
&\quad\left.+\,\frac{1}{B}\,\frac{\mathrm{d}^2B}{\mathrm{d}z^2}\,\gamma_{11}^6\right\}+\dot{P}_{11}\,\frac{1}{B}\,\frac{\mathrm{d}B}{\mathrm{d}z}\,\gamma_{11}^6\\
&\quad-\frac{1}{h_{11}}\left\{-\frac{\mathrm{d}\dot{A}_{11}^{\mathrm{e}}}{\mathrm{d}z}\,\gamma_{111}^{10}\,\frac{1}{B}\,\frac{\mathrm{d}B}{\mathrm{d}z}+\dot{C}_{11}\,\frac{1}{B}\,\frac{\mathrm{d}B}{\mathrm{d}z}\,\gamma_{111}^{11}\right.\\
&\quad\left.-\left[\dot{A}_{11}^{\mathrm{e}}\left(\frac{\mathrm{d}B}{\mathrm{d}z}\right)^2\gamma_{111}^5-\dot{C}_{11}B\,\frac{\mathrm{d}B}{\mathrm{d}z}\,\gamma_{111}^{12}\right]\right\}\\
&\quad-\frac{\mathrm{i}\sigma}{h_{11}\pi B}\,\frac{1}{N}\sum_{i=1}^{N}\left[-\left(\beta_{ri}-\rho_i\,\frac{\mathrm{d}B}{\mathrm{d}z}\,\beta_{zi}\right)\frac{1}{\mu_{11}\rho_i}\,J_1(\mu_{11}\rho_i)\right.\\
&\quad\left.-\,\mathrm{i}\beta_{\varphi i}J_1'(\mu_{11}\rho_i)\right]\frac{\exp\left[\mathrm{i}(\varphi_i-T_i)\right]}{\beta_{zi}}\,,
\end{aligned}$$

were the following notation is used: $z=\omega_0 z'/c=2\pi z'/\lambda_0$ is the normalized length, z' is the dimensional length, ω_0 is the reference frequency, $\dot{A}_{11}^{\mathrm{e}}=\dot{E}_{tm}^{\mathrm{e}}e/m_0c^2$, $\dot{E}_{tm}^{\mathrm{e}}$ is the complex amplitude of the transverse component of the electric intensity of the E_{11} wave; $\dot{C}_{11}=\dot{E}_{em}^{\mathrm{e}}e/\omega_0c$, $\dot{E}_{em}^{\mathrm{e}}$ is the complex amplitude of the longitudinal component of the electric intensity of the wave; $\dot{A}_{11}^{\mathrm{m}}=\dot{E}_{tm}^{\mathrm{m}}e/m_0c^2$, $\dot{E}_{tm}^{\mathrm{m}}$ is the complex amplitude of the transverse component of the electric intensity of the H_{11} wave;

$$\dot{V}_{111}=\frac{\mathrm{d}\dot{A}_{11}^{\mathrm{e}}}{\mathrm{d}z}-\nu_{11}\dot{C}_{11}\,,\quad \dot{P}_{111}=\frac{\mathrm{d}\dot{A}_{11}^{m}}{\mathrm{d}z}\,,$$

$$\gamma_{111}^{3}=\frac{\mu_{11}\nu_{11}J_0(\nu_{11})J_1(\mu_{11})}{\nu_{11}^2-\mu_{11}^2}\,,\quad \gamma_{111}^{-3}=\frac{\nu_{11}J_1(\mu_{11})J_0(\nu_{11})}{\mu_{11}(\mu_{11}^2-\nu_{11}^2)}\,,$$

$$\gamma_{111}^{4}=\frac{\mu_{11}J_1(\mu_{11})J_0(\nu_{11})}{\mu_{11}^2-\nu_{11}^2}\,,\quad \gamma_{111}^{5}=\frac{2\nu_{11}^2J_1(\mu_{11})J_0(\nu_{11})}{\mu_{11}(\mu_{11}^2-\nu_{11}^2)^2}\,,$$

$$\gamma_{s11}^{5}=J_1^2(\mu_{11})\left[\frac{1+\mu_{11}^2}{6}+\frac{1}{2\mu_{11}^2}\right],$$

$$\gamma_{11}^{6}=\frac{1}{h_{11}}\,\frac{1}{\mu_{11}^2}\,J_1^2(\mu_{11})\,,$$

$$\gamma_{111}^{10}=\frac{\mu_{11}}{\nu_{11}^2-\mu_{11}^2}\,J_0(\nu_{11})J_1(\mu_{11})\,,$$

$$\gamma_{111}^{11}=\mu_{11}\nu_{11}\,\frac{J_0(\nu_{11})J_1(\mu_{11})}{\nu_{11}^2-\mu_{11}^2}\,,$$

$$\gamma_{111}^{12}=\frac{\nu_{11}}{\mu_{11}(\mu_{11}^2-\nu_{11}^2)}\,J_0(\nu_{11})J_1(\mu_{11})\,,$$

$$e_{11}=\frac{1}{2}\,J_0^2(\nu_{11})\,,\quad h_{11}=\frac{1}{2}\,J_1^2(\mu_{11})\left(1-\frac{1}{\mu_{11}^2}\right),$$

J_0 and J_1 are the Bessel functions; $B(z)=\omega_0 b(z)/c$, $b(z)$ is the internal waveguide radius; $\sigma=|I_0|e\mu_0/cm_0=0.73723\times10^{-3}|I_0|$, I_0 is the beam current measured in amperes, μ_0 is the permeability of free space; $\varphi_i(z)$ is the azimuth of the ith particle at a section z; $T_i(z)=\omega_0 t_i(z)/c$, $t_i(z)$ is the time instant at which the ith particle passes through the current section z; $\rho_i(z)=r_i(z)/B(z)$; $\beta_{ri}(z)=V_{ri}(z)/c$, $\beta_{\varphi i}(z)=V_{\varphi i}(z)/c$, $\beta_{zi}(z)=V_{zi}(z)/c$ are the radial, phase, and longitudinal normalized electron velocities, respectively; $J_1(\nu_{11})=0$, ν_{11} is the first root of $J_1(x)$, $J_1'(\mu_{11})=0$, μ_{11} is the first root of $J_1'(x)$; and i labels the particle phase trajectory, $i=1,\ldots,N$.

The initial conditions for the system of equations (9) are given by

$$\operatorname{Im}\left\{\dot A_{11}^{\mathrm e}(0)\right\}=0\,,\quad \operatorname{Re}\left\{\dot A_{11}^{\mathrm e}(0)\right\}=\left|K_{\mathrm{in}}\,\frac{(1-R_0)\sigma\chi_{\mathrm e11}}{\pi mR_0e_{11}}\right|^{1/2},$$

where $K_{\mathrm{in}}=P_{\mathrm{in}}/(U_0|I_0|)$, P_{in} is the output power, U_0 is the accelerating voltage of the electron beam, and

$$\operatorname{Im}\left\{\dot A_{11}^{\mathrm m}(0)\right\}=0\,,\quad \operatorname{Re}\left\{\dot A_{11}^{\mathrm m}(0)\right\}=0\,,$$

$$\operatorname{Re}\left\{\dot V_{11}(0)\right\}=0\,,\quad \operatorname{Im}\left\{\dot V_{11}(0)\right\}=-\frac{1}{\chi_{\mathrm e11}}\operatorname{Re}\dot A_{11}^{\mathrm e}(0)\,,$$

$$\operatorname{Re}\left\{\dot P_{11}(0)\right\}=0\,,\quad \operatorname{Im}\left\{\dot P_{11}(0)\right\}=0\,,$$

$$\chi_{\mathrm m11}^2=1-\frac{\mu_{11}^2}{B^2(0)}\,,$$

$$\chi_{\mathrm e11}^2=1-\frac{\nu_{11}^2}{B^2(0)}\,,\quad R_0=\sqrt{1-\beta^2(0)}\,.$$

The reflection coefficient at the right end of the domain is defined as

$$\dot\Gamma^{\mathrm e}=-\frac{\mathrm d\dot A_{11}^{\mathrm e}(z_0)/\mathrm dz+\chi_{\mathrm e11}\dot A_{11}^{\mathrm e}(z_0)}{\mathrm d\dot A_{11}^{\mathrm e}(z_0)/\mathrm dz-\chi_{\mathrm e11}\dot A_{11}^{\mathrm e}(z_0)}\,,$$

$$\dot\Gamma^{\mathrm m}=-\frac{\mathrm d\dot A_{11}^{\mathrm m}(z_0)/\mathrm dz+\chi_{\mathrm m11}\dot A_{11}^{\mathrm m}(z_0)}{\mathrm d\dot A_{11}^{\mathrm m}(z_0)/\mathrm dz-\chi_{\mathrm m11}\dot A_{11}^{\mathrm m}(z_0)}\,. \tag{10}$$

The equations of motion of the ith charged particle in the field of the E_{11} and H_{11} waves of an irregular waveguide and an irregular magnetostatic field are

$$\frac{\mathrm d\beta_{xi}}{\mathrm dz}=-\frac{R_i}{\beta_{zi}}\left[\bar E_{xi}+\beta_{yi}(F+H_{zi})-\beta_{zi}(\bar H_{yi}+F_{yi})\right.$$
$$\left.-\beta_{xi}(\beta_{xi}\bar E_{xi}+\beta_{yi}\bar E_{yi}+\beta_{zi}\bar E_{zi})\right],$$

$$\frac{\mathrm d\beta_{yi}}{\mathrm dz}=-\frac{R_i}{\beta_{zi}}\left[\bar E_{yi}-\beta_{xi}(F+H_{zi})+\beta_{zi}(\bar H_{xi}+F_{xi})\right.$$
$$\left.-\beta_{yi}(\beta_{xi}\bar E_{xi}+\beta_{yi}\bar E_{yi}+\beta_{zi}\bar E_{zi})\right],$$

$$\frac{\mathrm d\beta_{zi}}{\mathrm dz}=-\frac{R_i}{\beta_{zi}}\left[\bar E_{zi}+\beta_{xi}(\bar H_{yi}+F_{yi})-\beta_{yi}(\bar H_{xi}+F_{xi})\right.$$
$$\left.-\beta_{zi}(\beta_{xi}\bar E_{xi}+\beta_{yi}\bar E_{yi}+\beta_{zi}\bar E_{zi})\right],$$

$$\frac{\mathrm dx_i}{\mathrm dz}=\frac{\beta_{xi}}{\beta_{zi}}\,,\quad \frac{\mathrm dy_i}{\mathrm dz}=\frac{\beta_{yi}}{\beta_{zi}}\,,\quad \frac{\mathrm dT_l}{\mathrm dz}=\frac{1}{\beta_{zi}}\,. \tag{11}$$

Here, the following notation is used:

$$R_i=\sqrt{1-\beta_{xi}^2-\beta_{yi}^2-\beta_{zi}^2}\,,\quad F(z)=\frac{\mu_0\eta_0H_z^0(z)}{\omega_0}\,,$$

$$F_{xi}=-\frac{r_i}{2}\,\frac{\mathrm dF}{\mathrm dz}\cos\varphi_i\,,\quad F_{yi}=-\frac{r_i}{2}\,\frac{\mathrm dF}{\mathrm dz}\sin\varphi_i\,,$$

$$r_i=\sqrt{x_i^2+y_i^2}\,,\quad \varphi_i=\operatorname{arctg}\left(\frac{y_i}{x_i}\right),$$

$$\bar E_{xi}+\mathrm i\bar E_{yi}=\frac{1}{2B}\left\{\dot A_{11}^{\mathrm e}J_0(\nu_{11}\rho_i)\exp(\mathrm iT_i)\right.$$
$$-\dot A_{11}^{\mathrm e}J_2(\nu_{11}\rho_i)\exp\left[\mathrm i(2\varphi_i-T_i)\right]-\dot A_{11}^{\mathrm m}J_0(\mu_{11}\rho_i)\exp(T_i)$$
$$\left.-\dot A_{11}^{\mathrm m*}J_2(\mu_{11}\rho_i)\exp\left[\mathrm i(2\varphi-T_i)\right]\right\},$$

$$\bar E_{zi}=\frac{1}{2}\left\{J_1(\nu_{11}\rho_i)\left(\dot C_{11}\exp\left[-\mathrm i(\varphi_i-T_i)\right]\right.\right.$$
$$\left.+\dot C_{11}^{*}\exp\left[\mathrm i(\varphi_i-T_i)\right]\right)-\frac{\rho_i}{B}\,\frac{\mathrm dB}{\mathrm dz}J_1'(\nu_{11}\rho_i)$$
$$\times\left(\dot A_{11}^{\mathrm e}\exp\left[-\mathrm i(\varphi_i-T_i)\right]+\dot A_{11}^{\mathrm e*}\exp\left[\mathrm i(\varphi_i-T_i)\right]\right)$$
$$-\frac{1}{\mu_{11}\rho_i}\,J_1(\mu_{11}\rho_i)\left(\dot A_{11}^{\mathrm m}\exp\left[-\mathrm i(\varphi_i-T_i)\right]\right.$$
$$\left.\left.+\dot A_{11}^{\mathrm m*}\exp\left[\mathrm i(\varphi_i-T_i)\right]\right)\right\},$$

$$\bar H_{xi}+\mathrm i\bar H_{yi}=\frac{1}{2B}\left\{\nu_{11}\left(\dot C_{11}J_0(\nu_{11}\rho_i)\exp(\mathrm iT_i)\right.\right.$$
$$\left.+\dot C_{11}^{*}J_2(\nu_{11}\rho_i)\exp\left[\mathrm i(2\varphi_i-T_i)\right]\right)$$
$$-\frac{\mathrm d\dot A_{11}^{\mathrm e}}{\mathrm dz}\,J_0(\nu_{11}\rho_i)\exp(\mathrm iT_i)-\frac{\mathrm d\dot A_{11}^{\mathrm e*}}{\mathrm dz}\,J_2(\nu_{11}\rho_i)$$
$$\times\exp\left[\mathrm i(2\varphi_i-T_i)\right]+\frac{1}{B}\,\frac{\mathrm dB}{\mathrm dz}\,\mu_{11}\rho_iJ_1(\mu_{11}\rho_i)$$
$$\left.\times\left(\dot A_{11}^{\mathrm m}\exp\left[-\mathrm i(\varphi_i-T_i)\right]+\dot A_{11}^{\mathrm m*}\exp\left[\mathrm i(\varphi_i-T_i)\right]\right)\right\},$$

$$\bar H_{zi}=\frac{1}{B^2}\left\{\mu_{11}J_1(\mu_{11}\rho_i)\left(\dot A_{11}^{\mathrm m}\exp\left[-\mathrm i(\varphi_i-T_i)\right]\right.\right.$$
$$\left.\left.+\dot A_{11}^{\mathrm m*}\exp\left[\mathrm i(\varphi_i-T_i)\right]\right)\right\}.$$

In the absence of the initial REF modulation, the initial conditions for the system of equations (11) can be specified as

$$\varphi_i(0) = 0\,,$$

$$\beta_{xi} = 0\,, \quad \beta_{yi}(0) = 0\,, \quad \beta_{zi}(0) = 0\,, \quad \beta_{z0} = \frac{\beta_0}{\sqrt{1+q^2}}\,,$$

$$x_i(0) = r_{vc}\,, \quad y_i(0) = 0\,, \quad T_i(0) = \frac{2\pi}{N}\,(i-1)\,. \tag{12}$$

In the notation adopted, the 'electron' efficiency is defined as

$$\eta_{\rm e}(z) = \frac{1}{N}\sum_{i=1}^{N}\frac{1 - R_0/R_i(z)}{1 - R_0}\,, \tag{13}$$

and the respective 'wave' efficiencies are of the form

$$\eta_E(z) = \frac{\pi R_0 e_{11}}{(1-R_0)\sigma}\,{\rm Im}\,(\dot{A}_{11}^{\rm e}\dot{V}_{11}^{*})\,,$$

$$\eta_H(z) = \frac{\pi R_0 h_{11}}{(1-R_0)\sigma}\,{\rm Im}\,(\dot{A}_{11}^{m}\dot{P}_{11}^{*})\,. \tag{14}$$

Based on the mathematical model formulated above, we derived and analyzed the versions of efficiency-optimized TWGs with a uniform magnetic field and a periodic corrugated waveguide. The waveguide profile was described by the function

$$B(z) = g_1 + g_2\sin^2\left(g_3\pi\,\frac{z}{z_0}\right),$$

where g_1, g_2, and g_3 are variable parameters.

Version 1. TWG with a thin electron flow ($r_{vc} = 0$): $\beta_0 = 0.8$, $F = 0.696$, $K_{\rm in} = 0.005$, $g_1 = 4.338$, $g_2 = 1.127$, $g_3 = 35$, $z_0 = 31.14$, $\sigma = 1.121$, efficiency$= \eta = \eta_{\rm e} = \eta_E + \eta_H = 0.97$.

Figure 13 shows the integral characteristics $\beta_z(z)$, $\eta(z)$, $\eta_E(z)$, and $\eta_H(z)$ of this version, as well as the waveguide profile $B(z)$.

Figure 14 depicts the electron trajectories in the transverse section for different numbers i (or different phases of the entry into the interaction region $\omega t_{i0} = 2\pi\,i/N$).

An analysis of the above results leads to the following conclusions:

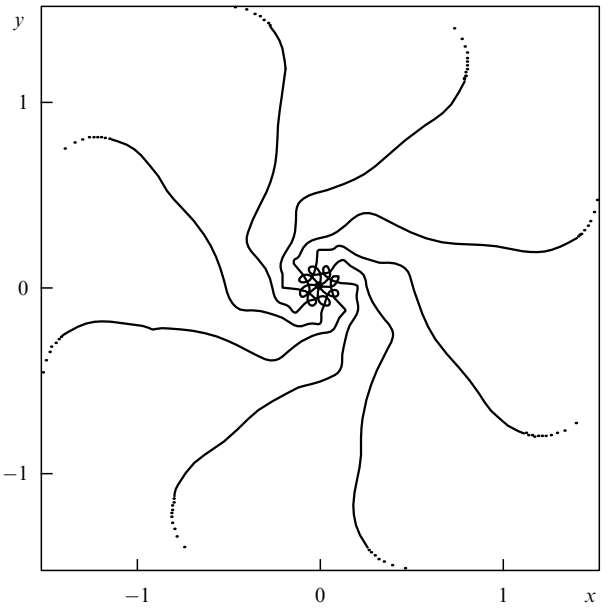

Figure 14. Electron trajectories in the transverse section for version 1 for different phases of the entry of the electrons into the waveguide.

(i) the overall efficiency $\eta(z_0)$ of the TWG with the combined interaction between an initially rectilinear REF and the coupled rotating modes EH_{11} and HE_{11} of the corrugated waveguide approaches 100%, as in a single-mode TWG [12]. On the other hand, the development of an output converter transforming the component EH_{11} to HE_{11} is not difficult (an example of the calculation of such a converter is given in Ref. [18]);

(ii) the transverse electron phase trajectories (see Fig. 14) are congruent, as in a single-mode TWG [12]. This is evidence of the retention of a perfect electron phasing mechanism (independence from the phase of entry) in the two-mode TWG as well;

(iii) the form of the dependences $\eta_E(z)$ and $\eta_H(z)$ (see Fig. 13) signifies that EH_{11} is partially transformed to HE_{11}, and vice versa. In the interaction with the REF in the case of a

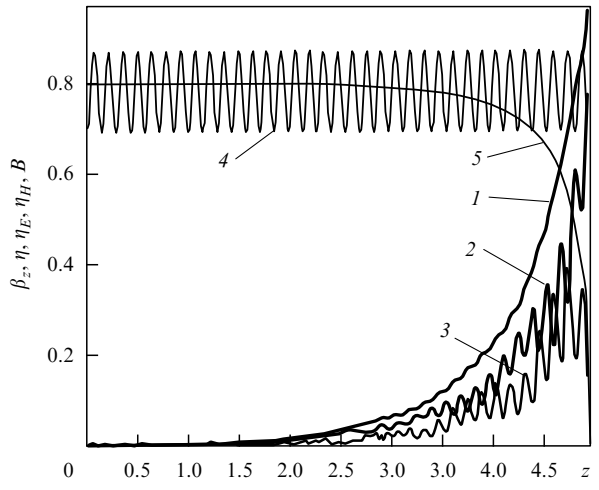

Figure 13. TWG characteristics (version 1): *1* — electron efficiency, *2* — E_{11} wave efficiency, *3* — H_{11} wave efficiency, *4* — waveguide profile $B(z)/2\pi$, *5* — average longitudinal electron velocity β_z.

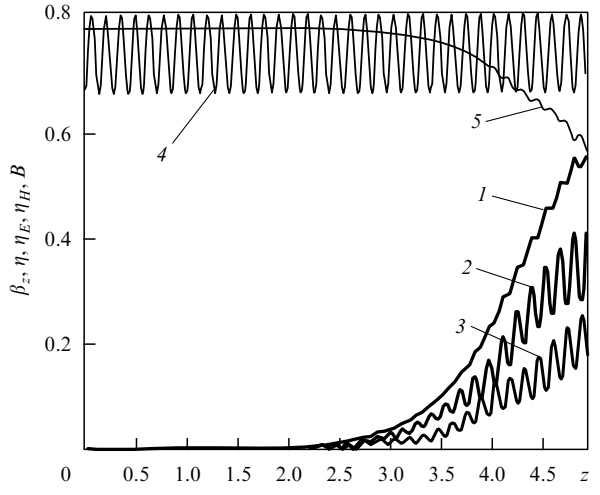

Figure 15. TWG characteristics (version 2): *1* — electron efficiency, *2* — E_{11} wave efficiency, *3* — H_{11} wave efficiency, *4* — waveguide profile $B(z)/2\pi$, *5* — average longitudinal electron velocity β_z.

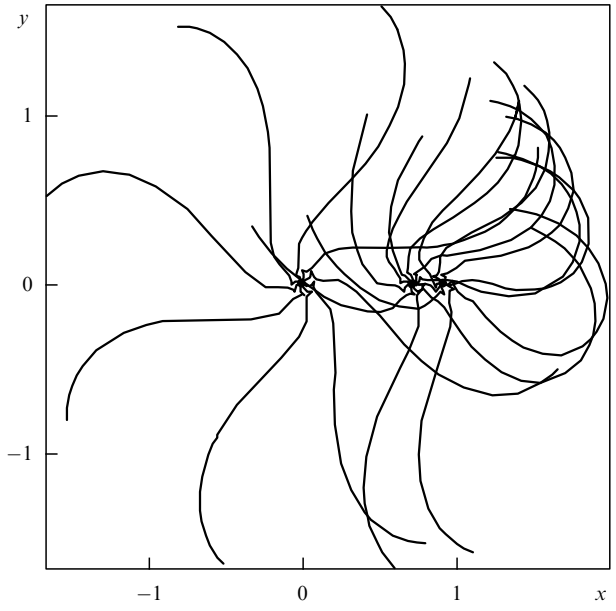

Figure 16. Transverse trajectories of the central and peripheral electrons of the beam for a three-layer model of version 2.

thin electron flow, the main role is played by the wave EH_{11}, which is subsequently transformed to the wave HE_{11}. Excluding the EH_{11} wave from consideration leaves the efficiency practically unchanged. Only the current and the value of the magnetostatic field somewhat change. This is explained by the fact that the phase velocities of the waves EH_{11} and HE_{11} are significantly different in a corrugated waveguide. The moderation is rather strong for the EH_{11} wave, but is insignificant for the HE_{11} wave because the waveguide radius for this wave is much greater than the critical one.

Version 2. TWG with a wide REF ($r_{vc} = 1$): $\beta_0 = 0.8$, $F = 0.541$, $g_1 = 4.263$, $g_2 = 0.969$, $g_3 = 35$, $z_0 = 31.14$, $\sigma = 1$, $K_{\text{in}} = 0.0008877$, efficiency $= \eta = \eta_{\text{e}} = \eta_E + \eta_H = 0.58$.

To calculate the TWG with a wide electron flow and a constant current density, the electron flow was divided into layers with the radii of guiding centers corresponding to equal areas of the electron rings. The number of rings was preset in a range between 3 and 7.

Figure 15 shows the integral characteristics and the dependence $B(z)$ for this version, and the phase trajectories of the central and peripheral electrons at the transverse section of the REF are plotted in Fig. 16.

The above results lead to the following conclusions:

(i) the character of the integral dependences $\beta_z(z)$, $\eta(z)$, $\eta_E(z)$, and $\eta_H(z)$ remains the same as for a thin REF, although the interaction efficiency is lower;

(ii) as can be seen from Fig. 16, the transverse trajectories of the peripheral REF electrons, unlike the trajectory of the central one, are entry-phase dependent;

(iii) the interaction efficiency decreases considerably less than in resonance gyrotons [8–10]. The TWG is therefore a substantially higher-frequency device than the resonance gyroton. For instance, if we proceed from the REF diameter 2.6 mm, the working wavelength for $r_{vc} = 1$ is $\lambda = 8$ mm.

Such a TWG superiority arises because an additional kind of interaction comes into effect for peripheral electrons — the Cherenkov interaction, which is similar to that occurring in the conventional TWT-O utilizing a corrugated waveguide. This is confirmed by the phase diagram in Fig. 17, which is indicative of a clearly defined longitudinal electron bunching. Naturally, this mechanism is absent in resonance gyrotons. Therefore, for peripheral electrons in the TWG utilizing a corrugated waveguide, there occurs a combined interaction mechanism — the Cherenkov–gyroton mechanism, which makes it possible to maintain a very high efficiency of the device.

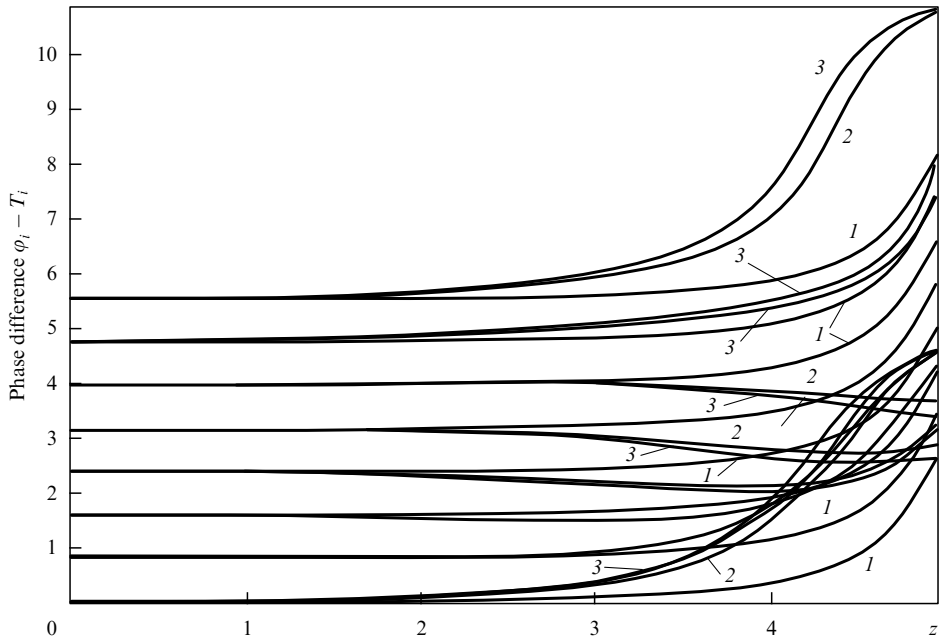

Figure 17. Phase diagram for a three-layer TWG model (version 2): *1* — phase trajectories of the central electrons; *2* — phase trajectories of the middle-layer electrons; *3* — phase trajectories of the electrons of the peripheral beam layer.

Version 3. Relativistic TWG with a wide REF ($r_{vc} = 1$): $\beta_0 = 0.9672$, $F = 1.063$, $g_1 = 4$, $g_2 = 0.866$, $g_3 = 35$, $z_0 = 31.14$, $\sigma = 1.06$, $K_{\text{in}} = 0.005$, efficiency $= \eta = \eta_{\text{e}} = \eta_E + \eta_H = 0.78$.

In this version, the device efficiency is significantly higher than the efficiency in version 2 — 78% against 58% — for the same radius of the electron flow. It is noteworthy that increasing the radius of the electron flow from $r_{vc} = 1$ to $r_{vc} = 3$ results in the reduction of the efficiency to 52%. In other words, even when the electron flow almost entirely fills the cross-sectional area of the waveguide ($r_{\max\,\text{wg}} = 3.8$), the efficiency does not decrease below 50%.

7. Conclusions

The results of investigations described in this paper show that the highly complicated optimization problem of the nonlinear interaction in Cherenkov-type devices has received an adequate solution. This solution was obtained in the works of our compatriot scientists based on the original methods of solving optimal control problems invoking the apparatus of atomic functions (see the Appendix). Highly representative in this respect are the materials on the advances in the area of TWT-O given in review [34]. The progress quite definitely correlates with the previous publication of Refs [17–23, 25, 28], etc. reporting the results on the optimization of spiral TWTs for efficiency and minimum nonlinear distortions. These papers reported the establishment of the optimum law of the cold phase velocity variation in the TWT interaction region and the elucidation of the character of optimum physical interaction processes in the optimized versions.

8. Appendix
Variational-iterative method for the solution of nonlinear optimal control problems

To avoid cumbersome mathematical manipulations, we choose a simplified version of an optimal control problem and make the following assumptions: a) the left end of phase trajectories moves freely over the given hypersurfaces; b) the right end of the trajectories is free (constraints are introduced into the overall functional — the goal function); c) the vectors of the state and control variables are continuous; and d) the interval of motion [0, T_0] is fixed. The fundamental points of the method explained with the example of such a problem are amply illustrated and extending the method to the general case presents no special problems [17, 18].

Under the conditions listed above, the optimal control problem is posed as follows (we illustrate the meaning of variables and parameters by the example of the problem of optimal control of the interaction process in microwave devices).

1. The mathematical model of the dynamic process is given in the form of a system of ordinary differential equations (equations of state)

$$\begin{aligned}&\frac{\mathrm{d}X_s}{\mathrm{d}T} \equiv X_s = f_s[X_1, X_2, \ldots, X_s, \ldots, X_n;\\ &g_1(T), \ldots, g_k(T);\ M_1, \ldots, M_l, T],\\ &s = 1, 2, \ldots, n, \quad 0 \leqslant T \leqslant T_0,\end{aligned} \tag{A.1}$$

or in the vector form,

$$\frac{\mathrm{d}\mathbf{X}}{\mathrm{d}T} = \dot{\mathbf{X}} = f[\mathbf{X}, \mathbf{g}(T), \mathbf{M}, T],$$

where $\mathbf{X} = (X_1, X_2, \ldots, X_n)^{\mathrm{T}}$ is the transposed n-dimensional vector of phase variables [coordinates (phases), velocities of the set of 'big particles' that simulate the electron flow, the amplitudes and phases of the force components of the electromagnetic field, and so forth]; $\mathbf{g}(T) = (g_1, g_2, \ldots, g_m)^{\mathrm{T}}$ is the m-dimensional interaction control vector (the T-distribution of the high-frequency and static fields, the profile of the waveguide system, the winding angle of the spiral SWS, etc.); $\mathbf{M}$ are the interaction control parameters (the amplitude and phase of the electromagnetic field in the resonator, the length of the interaction region, the working–cyclotron frequency mismatch, the beam current and diameter, the diameter of the waveguide or flight channel, etc.); and T is the reduced length of the interaction region or the reduced interaction time.

2. The boundary conditions are imposed at the left end for $T = 0$,

$$X_s(0) = X_s(\mathbf{B}), \tag{A.2}$$

where $\mathbf{B} = (B_1, \ldots, B_j, \ldots, B_C)^{\mathrm{T}}$ are the parameters of the initial conditions of the process.

3. The goal function is specified in the form of the functional (the Boltz problem)

$$J = \Phi\big(\mathbf{X}(T_0)\big) + \int_0^{T_0} f_{n+1}(\mathbf{X}, \mathbf{g}, \mathbf{M}, T)\,\mathrm{d}T. \tag{A.3}$$

We pose the following optimal control problem: among the continuous functions $X_s(T)$ $(s = \overline{1, n})$ and $g_k(T)$ $(k = \overline{1, m})$, to find those that satisfy Eqns (A.1) on the interval [0, T_0] and boundary conditions (A.2) for $T = 0$, and among the parameters $\mathbf{M}$ and $\mathbf{B}$, to find those that realize an extremum of functional (A.3).

We approximately represent the sought control function $g_k(T)$ as a finite series in the ordered, complete system of functions $\{\varphi_i(T)\}$ that are orthogonal on the interval $0 \leqslant T \leqslant T_0$ and satisfy the given constraints determined by the physical nature of controlling the interaction processes [17, 18],

$$g_k^N(T) = \sum_{i=1}^{N} A_{ki}\varphi_i(T). \tag{A.4}$$

Thus, after the problem in (A.1) and (A.2) is solved, functional (A.3) becomes a function of $n \times r$ parameters A_{ki}, and of the parameters $\mathbf{M}$ and $\mathbf{B}$. The maximum (minimum) of this function can be found using one of the methods for minimizing a function of several variables. When additional special constraints are imposed on the control function $g_k(T)$, in particular the smoothness conditions with the additional requirement that the higher derivatives should be small, each of the $\varphi_i(T)$ functions should also satisfy them. The functions derived and investigated in Refs [35–43] were found to satisfy all the aforementioned conditions. Furthermore, it can be shown that no other compact, infinitely differentiable functions have an equally good approximation capacity.

Among such functions, the simplest and best-studied is $\mathrm{up}(x)$ — the solution of the differential-functional equation

$$y'(x) = 2y(2x + 1) - 2y(2x - 1) \tag{A.5}$$

with the compact support [−1, 1], normalized by the condition $\int_{-1}^{1} \mathrm{up}(x)\,\mathrm{d}x = 1$.

The function $\mathrm{up}(x)$ has the integral representation

$$\mathrm{up}(x) = \frac{1}{2\pi}\int_{-\infty}^{+\infty} \exp(\mathrm{i}tx)F(t)\,\mathrm{d}t\,,$$

where

$$F(t) = \prod_{k=1}^{\infty} \frac{\sin(2^{-k}t)}{2^{-k}t}\,.$$

This even, infinitely differentiable function is not analytic at any point of its support $[-1, 1]$. Its Taylor series is a polynomial at binary-rational points (i.e., at the points of the form $2^{-k}k$) and has zero convergence radius at the other points of the support.

This function has the following properties: $\mathrm{up}(0) = 1$; it increases on $[-1, 0]$ and decreases on $[0, 1]$; for $x \in (0, 1)$, $\mathrm{up}(1 - x) = 1 - \mathrm{up}(x)$; and its integer-valued shifts are a partition of unity,

$$\sum_{k=-\infty}^{\infty} \mathrm{up}(x - k) = 1\,.$$

All the foregoing properties follow directly from Eqn (A.5).

The moments

$$a_{2k} = \int_{-1}^{1} x^{2k}\mathrm{up}(x)\,\mathrm{d}x\,, \quad b_k = \int_0^1 x^k \mathrm{up}(x)\,\mathrm{d}x$$

satisfy the recursive relations

$$a_0 = 1; \quad a_{2n} = \frac{(2n)!}{2^{2n} - 1}\sum_{k=1}^{n} \frac{a_{2n-2k}}{(2n-2k)!(2k+1)!}\,;$$

$$b_{2n+1} = \frac{1}{2^{2n+3}(n+1)}\sum_{k=0}^{n+1} a_{2n+2}\,.$$

At the points $k/2^n$, the function $\mathrm{up}(x)$ takes rational values. In particular,

$$\mathrm{up}(-1 + 2^{-n}) = \frac{b_{n-1}}{2^{C_n^2}(n-1)!}\,.$$

From Eqn (A.5), for the nth derivative $\mathrm{up}^{(n)}(x)$, we obtain

$$\mathrm{up}^{(n)}(x) = 2^{(2n+1)n/2}\sum_{k=1}^{2^n} \delta_k \mathrm{up}(2^n x + 2^n + 1 - 2k)\,,$$

where $\delta_1 = 1$, $\delta_{2k} = -\delta_k$, and $\delta_{2k-1} = \delta_k$.

Although the function $\mathrm{up}(x)$ is infinitely differentiable, the Taylor series is unsuitable for its calculation, because at every point $x_0 \in [-1, 1]$, it either has zero convergence radius or reduces to a polynomial (at the points $k/2^n$), and therefore does not converge to $\mathrm{up}(x)$. It is significant here that for an arbitrary n, there exist coefficients $C_k^{(n)}$ such that

$$x^n = \sum_{k=-\infty}^{\infty} C_k^{(k)}\mathrm{up}(x - k2^{-n})\,.$$

To evaluate $\mathrm{up}(x)$, use is made of the rapidly convergent series

$$\mathrm{up}(x-1) = \sum_{k=1}^{\infty}(-1)^{S_k+1}P_k \times \sum_{j=0}^{k} \frac{[2^{(j+1)^j-(k-j)(k-j-1)}/2]\,b_{k-j-1}}{(k-j-1)!\,j!}\,(x = 0, P_1, \ldots, P_k)\,,$$

$$0 \leqslant x \leqslant 1\,,$$

where b_l are the moments of $\mathrm{up}(x)$ for $l > 0$; $b_{-1} = 1$, $0! = 1! = 1$, $S_k = \sum_{j=1}^{k} P_j$; $(x = 0,\ P_1, \ldots, P_k)$ is the notation for the number x in the binary number system, i.e., $(x = 0, P_1 \ldots P_k) = x - 2^{-k}[2^k x]$; $[x]$ is the integer part of x; and $P_k = [2^k x] - 2[2^{k-1}x]$.

The residual term of this series satisfies the condition

$$|R_n| \leqslant \frac{1}{2^{n(n+1)/2}(n-1)!}\,.$$

Thus, we approximately represent the sought control function as

$$g_k^N(T) = \sum_{i=1}^{N} A_{ki}\,\mathrm{up}\left(\frac{T - T_{ki}}{\rho_{ki}}\right), \tag{A.6}$$

where T_{ki} is the shift parameter, $T_{ki}/\rho_{ki} \in [0, T_0]$, and ρ_{ki} is the width parameter of the $\mathrm{up}(z)$ function.

The methods for fast calculation of $\mathrm{up}(z)$ are given in Refs [35, 42, 43].

After substitution of expression (A.6) and after solution of the Cauchy problem in (A.1) and (A.2), functional (A.3) becomes a function of the $3N \times m$ parameters A_{ki}, T_{ki}, ρ_{ki}, and the parameters **M** and **B**. The minimum of this function can be found using the techniques for the minimization of functions of several variables. If gradient techniques are used for the minimization of J, it is possible to avoid the procedure of numerical (finite-difference) determination of the gradient of J [17, 18]. This technique is described below.

In view of condition (A.1) imposed on g_k and X_s (nonholonomic constraints), the optimal control problem posed above is a typical conditional extremum problem [17, 18], which can be expediently solved via the method of Lagrange multipliers. We introduce the yet undetermined Lagrange multipliers $\lambda_s(T)(s = \overline{1, n})$ and construct an auxiliary functional I,

$$I = J + \int_0^{T_0}\sum_{s=1}^{n} \lambda_s \varphi_s\,\mathrm{d}T\,,$$

where $\varphi_s = \dot{X}_s - f_s(X_s, g_k, M_i, T)$.

It is evident that if (A.1) is satisfied ($\varphi_s = 0$), I coincides with J. We introduce the Hamiltonian function

$$H = -f_{n+1} + \sum_{s=1}^{n} \lambda_s f_s = H(X_s, g_k, \lambda_s, M_i, T)\,,$$

then

$$I = \Phi\big(X_s(T_0)\big) + \int_0^{T_0}\left(\sum_{s=1}^{n} X_s\lambda_s - H\right)\mathrm{d}T. \tag{A.7}$$

We take the first variation of I

$$\delta I = \sum_{s=1}^{n}\frac{\partial \Phi}{\partial X_s}\,\delta X_s(T_0) + \int_0^{T_0}\left[\sum_{s=1}^{n}\left(\dot{X}_s\delta\lambda_s + \lambda_s\delta\dot{X}_s - \frac{\partial H}{\partial \lambda_s} - \frac{\partial H}{\partial X_s}\,\delta X_s\right) - \sum_{k=1}^{m}\frac{\partial H}{\partial g_k}\,\delta g_k - \sum_{i=1}^{l}\frac{\partial H}{\partial M_i}\,\mathrm{d}M_i\right]\mathrm{d}T \tag{A.8}$$

and perform the transformation

$$\int_0^{T_0} \lambda_s \delta \dot{X}_s \, \mathrm{d}T = \lambda_s \delta X_s \Big|_0^{T_0} - \int_0^{T_0} \dot{\lambda}_s \delta X_s \, \mathrm{d}T. \tag{A.9}$$

We also assume that Eqns (A.1) are exactly solved at each iteration, i.e., $\varphi_s = 0$, or

$$X_s - \frac{\partial H}{\partial \lambda_s} = 0 \qquad \left(\frac{\partial H}{\partial \lambda_s} = f_s \right).$$

It then follows that $\delta I = \delta J$, and we have

$$\begin{aligned} \delta J = &- \sum_{s=1}^{n} \lambda_s(0) \delta X_s(0) + \sum_{s=1}^{n} \left(\lambda_s(T_0) + \frac{\partial \Phi}{\partial X_s} \right) \delta X_s(T_0) \\ &- \int_0^{T_0} \left[\sum_{s=1}^{n} \left(\lambda_s + \frac{\partial H}{\partial X_s} \right) \delta X_s \right. \\ &\left. + \sum_{k=1}^{m} \frac{\partial H}{\partial g_k} \, \delta g_k + \sum_{i=1}^{l} \frac{\partial H}{\partial M_i} \, \mathrm{d}M_i \right] \mathrm{d}T. \end{aligned} \tag{A.10}$$

We extend the definition of $\lambda_s(T)$ as follows:

$$\lambda_s + \frac{\partial H}{\partial X_s} = 0; \tag{A.11}$$

$$\lambda_s(T_0) = - \frac{\partial \Phi}{\partial X_i(T_0)} \, . \tag{A.12}$$

With relations (A.2) and (A.6), we obtain

$$\begin{aligned} \delta X_s(0) &= \sum_{j=1}^{C} \frac{\partial X_s(0)}{\partial B_j} \, \mathrm{d}B_j \, , \\ \delta g_k^N &= \sum_{i=1}^{N} \left\{ \mathrm{up}\,(z_{ki}) \, \mathrm{d}A_{ki} - 2 \big[\mathrm{up}(2z_{ki} + 1) \right. \\ &\quad \left. - \mathrm{up}(2z_{ki} - 1) \big] \left(\frac{\mathrm{d}T_{ki}}{\rho_{ki}} + \frac{\mathrm{d}\rho_{ki} z_{ki}}{\rho_{ki}} \right) \right\}, \end{aligned} \tag{A.13}$$

where $z_{ki} = (T - T_{ki})/\rho_{ki}$.

The functional L now becomes just a function $J(A_{ki}, T_{ki}, \rho_{ki}, B_j, M_i)$. Accordingly, δJ becomes $\mathrm{d}J$ (i.e., the first variation of the functional J passes into the differential of the function J). We then obtain

$$\begin{aligned} \mathrm{d}J = &- \sum_{s=1}^{n} \sum_{j=1}^{C} \lambda_s(0) \, \frac{\partial X_{0s}}{\partial B_j} \, \mathrm{d}B_j \\ &- \int_0^{T_0} \left\{ \sum_{k=1}^{m} \frac{\partial H}{\partial g_k} \sum_{i=1}^{N} \left[\mathrm{up}(z_{ki}) \, \mathrm{d}A_{ki} - 2 \big[\mathrm{up}\,(2z_{ki} + 1) \right. \right. \\ &\left. - \mathrm{up}(2z_{ki} - 1) \big] \left(\frac{\mathrm{d}T_{ki}}{\rho_{ki}} + \frac{\mathrm{d}\rho_{ki} \, z_{ki}}{\rho_{ki}} \right) \right] \\ &\left. + \sum_{i=1}^{l} \frac{\partial H}{\partial M_i} \, \mathrm{d}M_i \right\} \mathrm{d}T. \end{aligned} \tag{A.14}$$

Expressions for the components of the gradient of J follow directly from relation (A.14):

$$\begin{aligned} &\frac{\partial J}{\partial B_j} = - \sum_{s=1}^{n} \frac{\partial X_{0s}}{\partial B_j} \, \lambda_s(0) \, , \quad j = \overline{1, C} \, ; \\ &\frac{\partial J}{\partial M_i} = - \int_0^{T_0} \frac{\partial H}{\partial M_i} \, \mathrm{d}T, \quad i = \overline{1, l} \, ; \\ &\frac{\partial J}{\partial A_{ki}} = - \int_{T_{ki} - \rho_{ki}}^{T_{ki} + \rho_{ki}} \frac{\partial H}{\partial g_k} \, \mathrm{up}\,(z_{ki}) \, \mathrm{d}T \, ; \\ &\frac{\partial J}{\partial T_{ki}} = \frac{2}{\rho_{ki}} \left[\int_{T_{ki} - \rho_{ki}}^{T_{ki}} \mathrm{up}\,(2z_{ki} + 1) \, \mathrm{d}T \right. \\ &\qquad \left. - \int_{T_{ki}}^{T_{ki} + \rho_{ki}} \mathrm{up}\,(2z_{ki} - 1) \, \mathrm{d}T \right]; \\ &\frac{\partial J}{\partial \rho_{ki}} = \frac{2}{\rho_{ki}} \left[\int_{T_{ki} - \rho_{ki}}^{T_{ki}} z_{ki} \, \mathrm{up}\,(2z_{ki} + 1) \, \mathrm{d}T \right. \\ &\qquad \left. - \int_{T_{ki}}^{T_{ki} + \rho_{ki}} z_{ki} \, \mathrm{up}\,(2z_{ki} - 1) \, \mathrm{d}T \right], \\ &k = \overline{1, m} \, ; \quad i = \overline{1, N} \, . \end{aligned} \tag{A.15}$$

Let a point $(B_j^{(n)}, M_i^{(n)}, A_{ki}^{(n)}, \rho_{ki}^{(n)})$ in the space of parameters under optimization be reached in the course of J minimization. Then the following operations are performed at the nth step of the iterative procedure for the solution of the given optimization problem:

(i) the system of equations (A.1) with boundary conditions (A.2) is solved with (A.6) taken into account for the specified parameter values;

(ii) the boundary conditions are determined for $\lambda_s(T_0)$ in accordance with (A.12);

(iii) systems of equations (A.1) and (A.11) are simultaneously solved from right to left (i.e., from T_0 to 0 in the variable T). Simultaneously determined in accordance with (A.15) are the components of the gradient of J, which are then used as the initial data for gradient minimization techniques defining the next $(n+1)$th point of the minimizing sequence in the space $(B_j, M_i, A_{ki}, T_{ki}, \rho_{ki})$. Among the gradient techniques, it is advisable to use the Gol'dfarb variable-metric technique [44, 45] as the most efficient as regards the rate of convergence and stability.

The proposed technique makes it possible to speed up the solution of the optimization problem by a factor of $(n+3)/4$ (n is the number of optimization parameters) in comparison with the conventional techniques that employ the finite-difference procedure to determine the gradient of the goal function.

References

1. Cherenkov P A *Dokl. Akad. Nauk SSSR* **2** 451 (1934) [*CR Acad. Sci. URSS* **2** 451 (1934)]
2. Tamm I E, Frank I M *Dokl. Akad. Nauk SSSR* **14** 107 (1937) [*CR Acad. Sci. URSS* **14** 107 (1937)]
3. Bolotovskiĭ B M *Usp. Fiz. Nauk* **62** 201 (1957)
4. Jelley J V *Cerenkov Radiation and Its Applications* (Moscow: IL, 1960) (Oxford: Pergamon Press, 1958) [Translated into Russian (Moscow: IL, 1960)]
5. Zrelov V P *Izluchenie Vavilova–Cherenkova i ego Primenenie v Fizike Vysokikh Energiĭ* Book 1 (Moscow: Atomizdat, 1968) [Translated into English: *Cherenkov Radiation in High-Energy Physics* Vol. 1 (Jerusalem: Israel Program for Scientific Translations, 1970)]
6. Zrelov V P *Izluchenie Vavilova–Cherenkova i ego Primenenie v Fizike Vysokikh Energiĭ* Book 2 (Moscow: Atomizdat, 1968) [Translated into English: *Cherenkov Radiation in High-Energy Physics* Vol. 2 (Jerusalem: Israel Program for Scientific Translations, 1970)]
7. Shestopalov V P (Ed.) *Generatory Difraktsionnogo Izlucheniya* (Generators of Diffraction Radiation) (Kiev: Naukova Dumka, 1991)
8. Kolosov S V, Kuraev A A *Radiotekh. Elektron.* **18** (12) (1973)

9. Kuraev A A *Radiotekh. Elektron.* **27** 1231 (1982)
10. Kuraev A A, Sinitsyn A K, Slepyan A Ya *Int. J. Electron.* **80** 603 (1996)
11. Kolosov S V et al. *Radiotekh. Elektron.* **44** (6) (1999) [*J. Commun. Technol. Electron* **44** 682 (1999)]
12. Kolosov S V, Kuraev A A, Sinitsyn A K *Elektromag. Volny Elektron. Sistemy* 5 (1) (2000)
13. Pierce J R *Traveling-Wave Tubes* (New York: Van Nostrand, 1950) [Translated into Russian (Moscow: Sov. Radio, 1971)]
14. Slater J C *Microwave Transmission* (New York: McGraw-Hill, 1942) [Translated into Russian (Moscow: Sov. Radio, 1948)]
15. Filimonov G F, Badlevskiĭ Yu N *Nelineĭnoe Vzaimodeĭstvie Elektronnykh Potokov i Radiovoln v LBV* (Nonlinear Interaction between Electron Flows and Radio Waves in a TWT) (Moscow: Sov. Radio, 1971)
16. Solntsev V A *Elektron. Tekhn. Ser. 1 Elektronika SVCh* (11) 87 (1971)
17. Kuraev A A *Moshchnye Pribory. Metody Analiza i Optimizatsii Parametrov* (High-Power Devices. Methods of Analysis and Parameter Optimization) (Moscow: Radio i Svyaz', 1986)
18. Kuraev A A, Baĭburin V B, Il'in E M *Matematicheskie Modeli i Metody Optimal'nogo Proektirovaniya SVCh-Priborov* (Mathematical Models and Methods of Optimum Design of Microwave Devices) (Minsk: Nauka i Tekhnika, 1990)
19. Kuraev A A, Soloveĭ M P *Radiotekh. Elektron.* **27** 1234 (1982)
20. Kuraev A A, Soloveĭ M P *Radiotekh. Elektron.* **28** 1339 (1983)
21. Kuraev A A, Soloveĭ M P, Slepyan G Ya *Radiotekh. Elektron.* **31** 118 (1986)
22. Polyak V E, Filatov V A *Radiotekh. Elektron.* **31** 2233 (1986)
23. Kuraev A A, Sinitsyn A K *Radiotekh. Elektron.* **34** 1264 (1989)
24. Kuraev A A, Sinitsyn A K *Radiotekh. Elektron.* **34** 2166 (1989)
25. Gurinovich A B, Kuraev A A, Sinitsyn A K *Elektromag. Volny Elektron. Sistemy* 5 (4) 34 (2000)
26. Kats A M, Il'ina E M, Man'kin N A *Nelineĭnye Yavleniya v SVCh-Priborakh O-Tipa s Dlitel'nym Vzaimodeĭstviem* (Nonlinear Effects in O-Type Microwave Devices with a Long Interaction) (Moscow: Sov. Radio, 1975)
27. Kats A M, Kudryashov V P, Trubetskov D I *Signal v Lampakh s Begushcheĭ Volnoĭ* (Signal in Traveling-Wave Tubes) (Saratov: Izd. Saratovskogo Univ., 1988)
28. Kuraev A A, Sinitsyn A K *Zarubezh. Radioelektron. Usp. Sovremennoĭ Radioelektron.* (1) 61 (1997)
29. Kuraev A A, Kuraev N A, Sinitsyn A K *Radiotekh. Elektron.* **39** (2) 26 (1994)
30. Kuraev A A, Sinitsyn A K *Radiotekh. Elektron.* **43** 1384 (1998)
31. Taranenko Z I, Trokhimenko Ya K *Zamedlyayushchie Sistemy* (Slow-Wave Systems) (Kiev: Tekhnika, 1965)
32. Angot A *Compléments de Mathématiques à l'Usage des Ingénieurs de l'Électrotechnique et des Télécommunications* 2nd ed. (Paris: Editions de la Revue d'Optique, 1962)
33. Navrotskiĭ A A, Sinitsyn A K *Radiotekh. Elektron.* **40** 1696 (1995)
34. Abrams R H et al. *IEEE Microwave Mag.* **2** (3) 61 (2001)
35. Kravchenko V F, Rvachev V L, Rvachev V A *Dokl. Akad. Nauk SSSR* **306** (1) 78 (1989) [*Sov. Phys. Dokl.* **34** 58 (1989)]
36. Kravchenko V F, Rvachev V L, Rvachev V A *Radiotekh. Elektron.* **40** 1385 (1995)
37. Kravchenko V F *Lektsii po Teorii Atomarnykh Funktsiĭ i Nekotorym ikh Prilozheniyam* (Lectures on the Theory of Atomic Functions and on Some of their Applications) (Moscow: IPRZhR, 2003)
38. Gulyaev Yu V, Kravchenko V F, Rvachev V A *Dokl. Ross. Akad. Nauk* **342** 29 (1995) [*Dokl. Math.* **51** 456 (1995)]
39. Kravchenko V F, Basarab M A *Buleva Algebra i Metody Approksimatsii v Kraevykh Zadachakh Elektrodinamiki* (Boolean Algebra and Approximation Techniques in Boundary-Value Problems of Electrodynamics (Moscow: Fizmatlit, 2004)
40. Kravchenko V F, Rvachev V A *Zarubezh. Radioelektron. Usp. Sovremennoĭ Radioelektron.* (4) 3 (1996)
41. Kravchenko V F, Rvachev V A, Pustovoit V I *Dokl. Ross. Akad. Nauk* **351** 16 (1996) [*Dokl. Math.* **54** 846 (1996)]
42. Kravchenko V F, Rvachev V A *Zarubezh. Radioelektron. Usp. Sovremennoĭ Radioelektron.* (8) 6 (1996)
43. Kravchenko V F *Zarubezh. Radioelektron. Usp. Sovremennoĭ Radioelektron.* (8) 23 (1996)
44. Gol'dfarb D *SIAM J. Appl. Math.* **17** 739 (1969)
45. Gol'dfarb D *Math. Comput.* **24** 23 (1970)